EXTRACTION OF SEMICONDUCTOR LASER RATE EQUATION PARAMETERS FOR SIMULATION OF FIBER-OPTICAL COMMUNICATION SYSTEM PURPOSE

EXTRACTION OF SEMICONDUCTOR LASER RATE EQUATION PARAMETERS FOR SIMULATION OF FIBER-OPTICAL COMMUNICATION SYSTEM PURPOSE

BY

YE FENG WEN, B.ENG.

A THESIS

SUBMITTED TO THE DEPARTMENT OF ELECTRICAL & COMPUTER ENGINEERING

AND THE SCHOOL OF GRADUATE STUDIES

OF MCMASTER UNIVERSITY

IN PARTIAL FULFILMENT OF THE REQUIREMENTS

FOR THE DEGREE OF

MASTER OF APPLIED SCIENCE

Master of Applied Science (2012) McMaster University

(Electrical & Computer Engineering) Hamilton, Ontario, Canada

TITLE:	EXTRACTION OF SEMICONDUCTOR LASER RATE EQUATION PARAMETERS FOR SIMULATION OF FIBER-OPTICAL COMMUNICATION SYSTEM PURPOSE
AUTHOR:	Ye Feng Wen B.ENG., (Electrical Engineering) McMaster University, Hamilton, Canada
SUPERVISOR:	Dr. Wei-Ping Huang
NUMBER OF PAGES:	xiv, 86

To those who I loved and loved me

Abstract

This thesis presents the methods to extract modal parameters of semiconductor laser diodes based on a general zero-dimensional rate equation model. Three experiments, namely: the steady-state power versus injection current, small signal intensity modulation response and measurement of small signal response through dispersive optical fiber have been introduced, performed and analyzed under a sample space of 20 Multiple Quantum Well (MQW) Distributed feedback (DFB) laser of the same specification and from the same manufacturer. Testing software has been developed to perform the experiments , collect and analyze the data. The test results display an interesting Gaussian distributions that can be used to enhance further extraction process.

An new method to extract the line-width enhancement factor has been purposed, which introduce a new way to extract rate equation parameters for laser lasing at the wave length for zero dispersion in optical fiber ($1310nm$). The new method circumvent the difficulty for measurement of small signal response through dispersive optical fiber method will not work due to the low fiber dispersion around this wavelength. This method has been validated and published at OSA conference.

Acknowledgments

I would like to take this chance to thank everyone who loves me, who I love in all parts of my journey in life.

I would like to sincerely thank my supervisor Dr. Wei-Ping Huang for his encouragement, guidance and support through my graduate study. I can't forget all these discussion with him, intuitive, inspiriting and supportive. Without him, I won't have chance of exposure myself under this new field of study and experience in fabulous research life in these two years.

I would like to thank Dr. Xun Li and Dr. Shiva Kumar for great lectures on fiber-optical communication system topics.These memory will persist not just in terms of knowledge, but also as these professionalism of them in academic and great character in life.

I would like to thank Dr. Lin Han for all his help, academic-wise or life-wise, and excellent co-work together in research. Working with him making lengthy time in lab a more fun experience.

I would also want to thanks all my friends at McMaster, Yunfei Cai, Haibo Liang, Tingxia Li, Xiaojun Liang, Jing Shao, Lanxing Deng, Kan He,Shiwei Bao,Yajun Wang, Ying Zhang, Qingyi Guo, Yu Zhang, Sheng Tu, Wilson Song and Na He who share their life in these two years with me, happiness or sadness. I can't imagine

how can I go thought these days without you guys. And I will miss the time we had together.

Last but not least, I would like to thank my family- my wife, my mother, my parents in law and my son - for all these years of love, sacrifice and support. You are the reasons of my life.

Notation and abbreviations

Γ	mode confinement factor(unitless)
N_0	Carrier density at transparency (m^{-3})
τ_p	photon life time (s)
β_{sp}	fraction of spontaneous emission coupled into lasing mode (unitless)
τ_c	carrier lifetime (s)
V_{act}	active layer volume (m^3)
g_0	gain slope constant (m^3/s)
ϵ	gain compression factor (m^3)
η	differential quantum efficiency (unitless)
α	line-width enhancement factor (unitless)
$N(t)$	electron density (m^{-3})
$S(t)$	photon density (m^{-3})
$I(t)$	injection current (A)
q	electron charge (C)
h	Planck's constant ($J \cdot s$)
v	unmoderated optical frequency (Hz)
v_g	group velocity (m/s)

A	non-radiative recombination coefficient (unitless)
B	radioactive recombination coefficient (unitless)
C	Auger recombination coefficient (unitless)
η_i	quantum efficiency (unitless)

Contents

List of Figures

List of Tables

Chapter 1

Introduction

1.1 Fiber-Optic Communication System

A communication system transmits information from one place to another, whether separated by a few kilometers or by oversea distances. Information is often carried by an electromagnetic carrier wave whose frequency can vary from a few megahertz to several hundred terahertz. Optical communication systems use high carrier frequencies (100 THz) in the visible or near-infrared region of the electromagnetic spectrum. Fiber-optic communication systems are light-wave systems that employ optical fibers for information transmission. Such systems have been deployed worldwide since 1980 and have indeed revolutionized the technology behind telecommunications [1]. The main components of Fiber-optic Communication systems are optical transmitters, optical receivers, optical fibers and optical amplifiers. As figure 1.1 shows a basic fiber-optic communication system with these components.

The role of the optical transmitter is to convert an electrical input signal into the corresponding optical signal and then launch it into the optical fiber serving as

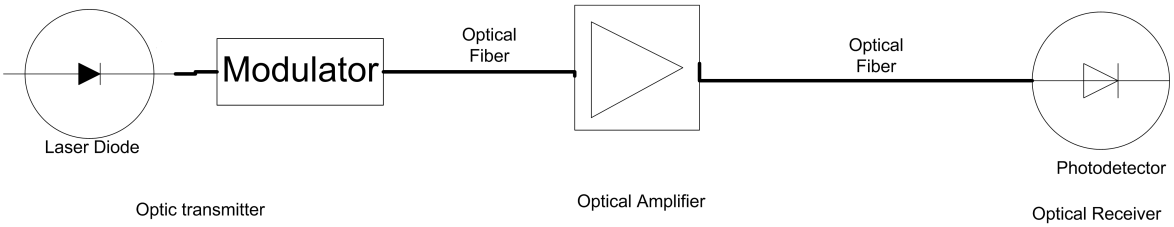

Figure 1.1: A basic fiber-optic communication system: with optical transmitters, optical receivers, optical fibers and optical amplifier.

a communication channel[2]. The major component of the optical transmitters is an optical source. Fiber-optic communication systems often use semiconductor optical sources such as light-emitting diodes (LEDs) and semiconductor lasers because of several inherent advantages such as compact size, high efficiency, good reliability, right wavelength range, small emission area compatible with fiber-core dimensions.

The role of an optical receiver is to convert the optical signal back into electrical form and recover the data transmitted through the light-wave system. Its main component is a photo-detector that converts light into electricity through the photo-electric effect. The requirements for a photo-detector are similar to those of an optical source. It should have high sensitivity, fast response, low noise, low cost and high reliability. Its size should be compatible with the fiber-core size, These requirements are best met by photo-detectors made of semiconductor materials.

The phenomenon of total internal reflection, responsible for guiding of light in optical fibers, has been know since 1854. Although glass fibers were made in 1920s, their use became practical only in 1950s, when the use of a cladding layer led to considerable improvement in their guiding characteristics. Before 1970, optical fibers were used mainly for medical imaging over short distances. Their use for communication

purposes was considered impractical because of high losses. However, the situation changed drastically in 1970 when the loss of optical fibers was reduced to below 20 dB/km[3]. Further progress resulted by 1979 in a loss of only 0.2 dB/km near the 1.55-μm spectral region[4]. The availability of low-loss fibers led to a revolution in the field of light-wave technology and started the era of fiber-optic communications [1].

The transmission distance of any fiber-optic communication system is eventually limited by fiber losses. For long-haul systems, the loss limitation has traditionally been overcome using optoelectronic repeaters in which the optical signal is first converted into an electrical current and then regenerated using a transmitter. Such regenerators becomes quite complex and expensive for wavelength-division multiplexed (WDM) light-wave systems. An alternative approach to loss management makes use of optical amplifiers, which amplify the optical signal directly without requiring its conversion to the electrical domain. Several kinds of optical amplifiers were developed during the 1980s, and the use of optical amplifiers for long-haul light-wave systems became widespread during the 1990s. By 1996, optical amplifier were a part of the fiber-optic cables laid across the Atlantic and Pacific oceans [1].

1.2 Distributed Feedback Semiconductor Laser

Distributed feedback (DFB) is a type of laser diode where the active region of the device is periodically structured as a diffraction grating.[5][6][7] The structure builds a one dimensional interference grating and the grating provides optical feedback for the laser. The grating acts as the wavelength selective element which reflect only a narrow band of wavelengths, thus produce a single longitudinal lasing mode. Which in contrast to a Fabry-Perot laser[8], where the facets of the chip form the two mirror

and provide feedback that a broadband of wavelengths are reflected to cause multiple longitudinal modes.

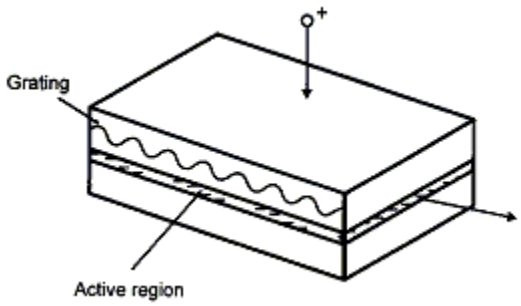

Figure 1.2: A simple structure of Distributed Feedback (DFB) semiconductor laser.

In long-haul fiber-optic communication system, Distributed feedback (DFB) semiconductor lasers plays the major role as optical transmitter. Due to its short spectral width and stability over other type of laser. In fact, the deploy of the 3rd generation light-wave system s was possible only after the development of DFB semiconductor lasers, which reduce the impact of fiber dispersion by reducing the source spectral width below 100 MHz.

1.3 Simulation of Fiber-Optical Communication System

In a long-haul fiber-optic communication system design, many things need to be take into account before deploy, such as loss, dispersion and nonlinearity of the fiber, bit rate, transmission distance, power budgets (or link budget), rise-time budgets (or bandwidth budget) and etc.[9] With the rise of computing technique and relative

price of computer hardware become lower, the use of simulation of the fiber-optic communication system prior to the deployment in design phase become more and more popular. Which are greatly reduce the cost and time consumption than setup experiment to design and verify the entire process. The process can be even done on a regular personal computer in acceptable time to achieve fine result. During computer simulation, the parameters can be modified and verified whether it matches required specifications.

As previous section's discussion, the DFB laser is one of the key components in light-wave communication systems. The single mode property of the DFB laser significantly reduced the chromatic dispersion of light-wave signal in the optical fiber compared with the multi-mode lasers such as the Fabry-Perot laser. Due to the low dispersion characteristic, the DFB lasers are widely used in the long haul communication. It has attached a lot of attentions from researches in these years. A lot of works have been done in studying the properties of existing DFB lasers, employing new materials and designing new structures to improve the performance in high speed communication systems.

Techniques in DFB laser simulation includes 2D and 3D physical base behavior modeling which are more precise and provide high accuracy to the physics of the device.[10][11][12][13] However, the drawback of these methods are also manifest. Since these methods focus on the detail physics and structures of the device, thus, the use of memory and the amount of time that consumed by these methods are not acceptable for the system-wide simulation. There are some fine detail that is generated by these method are not significant in the entire system simulation. Thus, the use of transmitter simulation tool need to be simply enough that take less computational

power but also representing the main functionality of the laser.

The operating characteristics of semiconductor lasers are well described by a set of rate equations that govern the interaction of photons and electrons inside the active region. Zero dimensional (0-D) semiconductor rate equation methods are used for the purpose of fiber-optical communication system simulations. The simple yet accurate enough model is highly demanded for modeling the DFB laser as a light-wave source in a communication system. Behavior models for laser diodes have been very successful for efficient and accurate simulation of system performance of laser diodes with proper choice of model parameters. The single mode rate equation model is one behavior model very suitable to model the DFB laser with the advantages of simplicity, fast and accurate, etc.

1.4 Extraction of Semiconductor Laser Rate Equation Parameters

To estimate the performance of light-wave communication system, a rate equation description of the semiconductor laser is often used. Thus, the accuracy of semiconductor laser rate equation parameters is important for simulation of large system before depletion. Unfortunately, the information provide by the laser manufacture is often insufficient.Therefore, the extraction of semiconductor laser rate equation parameters is required[14][15].

In this thesis, few experimental methods has been introduced to extract DFB semiconductor rate equation parameters. As well as compared simulation result to experiment. In chapter two, the 0-D DFB laser rate equation mode is introduced along

with simulation result. The Parameter extraction methods and the experiments of 0D rate equation model for DFB are introduce in chapter three. In chapter four, a new method has been proposed to extract line-width enhancement factor (the α parameter).The conclusion and future work has been summarized in chapter five.

My contributions are:

1. Perform semiconductor laser rate equation parameters extraction experiment with a group of devices and observe their property.

2. Purpose a new method to extract line-width enhancement factor which is suitable to extract parameters for laser that is lasing at $1310nm$.

Chapter 2

Zero Dimensional for DFB Semiconductor Laser Rate Equations and Simulation

The DFB laser is one of the key components in light-wave communication systems. The single mode property of the DFB laser significantly reduced the chromatic dispersion of light-wave signal in the optical fiber compared with the multi-mode lasers such as the Fabry-Perot laser. Due to the low dispersion characteristic, the DFB lasers are widely used in the long haul communication. It has attached a lot of attentions from researches in these years. A lot of works have been done in studying the properties of existing DFB lasers, employing new materials and designing new structures to improve the performance in high speed communication systems..Of all methods, Zero dimensional (0-D) semiconductor rate equation methods are used for the purpose of fiber-optical communication system simulations. The simple yet accurate enough model is highly demanded for modeling the DFB laser as a light-wave source in a communication system. Behavior models for laser diodes have been very successful for efficient and accurate simulation of system performance of laser diodes with proper choice of model parameters. The single mode rate equation model is

one behavior model very suitable to model the DFB laser with the advantages of simplicity, fast and accurate, etc.

In this chapter, semiconductor laser rate equations of various type are introduced, as well as simulation of DFB laser based on 0D laser rate equations. In section 2.1 and 2.2, semiconductor laser rate equations of various type and their parameters are introduced. In section 2.3, the formulation for optical power is derived. In section 2.4, the steady state power versus injection current relationship is derived. In section 2.5, introduced the turn on delay formula is derived. In section 2.6, the small signal intensive modulation formula is derived. And in section 2.7, the formula of small signal intensive modulation through dispersive fiber is derived.

2.1 Large signal single mode rate equations

The large signal single mode rate equations are a set of coupled ordinary differential equations that described relationship between carrier density N and photon density S are written as the following form[16][17][18]:

$$\frac{dN(t)}{dt} = \frac{I(t)}{qV_{act}} - \frac{N(t)}{\tau_c} - g_0 \frac{N(t) - N_0}{1 + \epsilon S(t)} S(t) \ , \tag{2.1}$$

$$\frac{dS(t)}{dt} = \Gamma g_0 \frac{N(t) - N_0}{1 + \epsilon S(t)} S(t) - \frac{S(t)}{\tau_p} + \frac{\Gamma \beta_{sp} N(t)}{\tau_c} \ . \tag{2.2}$$

In addition, the phase and optical power are described as:

$$\frac{d\phi(t)}{dt} = \frac{\alpha}{2} \left(\Gamma g_0 (N(t) - N_0) - \frac{1}{\tau_p} \right) \tag{2.3}$$

Table 2.1: List of parameters to be extracted

Γ	mode confinement factor
N_0	Carrier density at transparency
τ_p	photon life time
β_{sp}	fraction of spontaneous emission coupled into lasing mode
τ_c	carrier lifetime
V_{act}	active layer volume
g_0	gain slope constant
ϵ	gain compression factor
η	differential quantum efficiency
α	line-width enhancement factor

and

$$p(t) = \frac{S(t)V\eta h\nu}{2\Gamma\tau_p} \ . \tag{2.4}$$

The above model is used for single mode laser for system simulation purposes [19]. Note that in some paper $\frac{1}{1+\epsilon S(t)}$, the gain compression term, maybe substituted with $1+\epsilon S(t)$ or $\frac{1}{1+\epsilon S(t)^{(}1/2)}$. However, $\frac{1}{1+\epsilon S(t)}$ agrees best with numerical solutions when more comprehensive models even for large photon density. And for small photon densities, all forms appear to be identical [20]. The gain slope constant is given by $g_0 = v_g a_0$, where v_g is the group velocity. Table 2.1 lists these parameters to be extracted.

2.2 Alternative form of rate equations

Alternatively, the rate equation can be written as:

$$\frac{dN(t)}{dt} = \frac{\eta_i I(t)}{qV_{act}} - R_{sp} - v_g a_0 \frac{N(t) - N_t}{1 + \epsilon S(t)} S(t) \ , \tag{2.5}$$

$$\frac{dS(t)}{dt} = \Gamma v_g a_0 \frac{N(t) - N_t}{1 + \epsilon S(t)} S(t) - \frac{S(t)}{\tau_p} + \frac{\Gamma \beta B N(t)^2}{\tau_n} \ . \tag{2.6}$$

where the carrier recombination rate is modeled as:

$$R_{sp} = AN(t) + BN(t)^2 + CN(t)^3 \tag{2.7}$$

in stand of $\frac{N(t)}{\tau_n}$ [21], where A is the non-radiative recombination coefficient, B is radioactive recombination coefficient, C is Auger recombination coefficient and η_i is quantum efficiency

2.3 Derivations of optical power

In the laser cavity, the photons lose in two ways due to the internal loss and the mirror loss. The internal loss is caused by the light material interaction. The mirror loss is expressed by

$$\alpha_{mirr} = \frac{1}{2L} \ln \left(\frac{1}{R_1 R_2} \right) \tag{2.8}$$

with L as length of the cavity and R_1 , R_2 as the reflectivity of the left and right facet, respectively. The photon lifetime is determined by the cavity loss and the mirror loss as

$$\tau_p = (v_g(\alpha_{in} + \alpha_{mirr}))^{-1} = \left(v_g \left(\alpha_{in} + \frac{1}{2L} \ln \left(\frac{1}{R_1 R_2} \right) \right) \right)^{-1} \tag{2.9}$$

where v_g is the group velocity of light in the cavity; α_{in} and α_{mirr} are the internal loss and mirror loss, respectively.

The laser diodes only lase when the injection current is larger than a threshold current. Before the threshold, the carriers will accumulate in the laser cavity but no

light comes out. An expression for the threshold current can be derived from the rate equation (2.1) and (2.2).At threshold or in steady-state, both $\frac{dN(t)}{dt}$ and $\frac{dS(t)}{dt}$ are zero, yet photon density is zero, (2.1) can be simplify to

$$\frac{I_{th}}{qV_{act}} - \frac{N_{th}}{\tau_c} = 0 \tag{2.10}$$

where I_{th} is the threshold current and N_{th} is the threshold carrier density.

By rearranging the above equation (2.10), one obtains

$$I_{th} = \frac{qV_{act}}{\tau_c} N_{th} \ . \tag{2.11}$$

Equation (2.2) can also be simplified by neglecting the spontaneous emission

$$\left(\frac{\Gamma g_0 (N_{th} - N_0)}{1 + \epsilon S} - \frac{1}{\tau_p} \right) S = 0 \ , \tag{2.12}$$

which can be rearranged to

$$N_{th} = N_0 + \frac{1 + \epsilon S}{\tau_p \Gamma g_0} \tag{2.13}$$

At the threshold, the photon density is very small. Therefore ϵS can be neglected,

$$N_{th} = N_0 + \frac{1}{\tau_p \Gamma g_0} \ . \tag{2.14}$$

Substituting (2.14) into (2.11) , the threshold current is derived as

$$I_{th} = \frac{qV_{act}}{\tau_c} \left(N_0 + \frac{1}{\tau_p \Gamma g_0} \right) \ , \tag{2.15}$$

when the threshold current is known, the photon density above the threshold can be

calculated by a simple expression containing the injection current and the threshold current. Because, above the threshold, the carrier density is locked at threshold current, and the spontaneous emission can be neglected, the carrier and photon rate equations can be simplified as

$$\frac{I}{qV} - \frac{N_{th}}{\tau_c} - \frac{g_0(N - N_0)}{1 + \epsilon S} S = 0 \ , \tag{2.16}$$

$$\frac{\Gamma g_0(N - N_0)}{1 + \epsilon S} S - \frac{S}{\tau_p} \ . \tag{2.17}$$

By rearrange equation (2.17)

$$\frac{\Gamma g_0(N - N_0)}{1 + \epsilon S} S = \frac{S}{\tau_p} \tag{2.18}$$

substituted (2.18) and (2.11) into (2.16) yield:

$$\frac{I}{qV_{act}} - \frac{I_{th}}{qV_{act}} - \frac{S}{\Gamma \tau_p} = 0 \ . \tag{2.19}$$

Therefore, by rearranging the above equation, the photon density above threshold is expressed by:

$$S = \frac{\Gamma \tau_p}{qV_{act}} (I - I_{th}) \ . \tag{2.20}$$

The output power from the two facets of a laser diode is related with the photo density in the cavity by the equation:

$$P = E \times v_g \times n \times \alpha_{mirr} \ , \tag{2.21}$$

where E is Photon energy which can be expressed as $\eta h v$; Photon speed as v_g; n

is photon number and express as: $S \times \frac{V_{act}}{\Gamma}$ and mirror loss as α_{mirr}.Therefore, the output power can be expressed as:

$$\begin{aligned} P(t) &= \eta h v \times v_g \times \left(S \times \frac{V_{act}}{\Gamma} \right) \times \alpha_{mirr} \\ &= \eta h v \times v_g \times \frac{V_{act}}{\Gamma} \times \frac{1}{2L} \ln \left(\frac{1}{R_1 R_2} \right) \times S \ , \end{aligned} \tag{2.22}$$

where h is the Planck's constant , v is the light-wave frequency and η is the differential quantum efficiency.

In most cases, the internal loss is far smaller than that of mirror loss, which means, α_{in} can be neglected. Then (2.9) can be reduce to:

$$\frac{1}{\tau_p} = v_g \times \alpha_{mirr} \ . \tag{2.23}$$

Then, substitute (2.9) into (2.22), output power can be expressed as:

$$P(t) = \frac{\eta h v V_{act}}{\Gamma \tau_p} S = \frac{\eta h c V_{act}}{\Gamma \tau_p \lambda} S \ , \tag{2.24}$$

where λ is the light-wave wavelength By substitute (2.20) into (2.24), the above threshold output power is expressed as a function of biased current:

$$P(t) = \frac{\eta h c}{q \lambda} (I - I_{th}) \ . \tag{2.25}$$

If the two facets have the same reflection coefficient, output power from each facet is given by

$$P_{left} = P_{right} = \frac{\eta h c V_{act}}{2 \Gamma \tau_p \lambda} S \tag{2.26}$$

or otherwise

$$P = P_{left} + P_{right} = \frac{hcv_g V_{act} S}{2L\lambda\Gamma} \ln\left(\frac{1}{R_1}\right) + \frac{hcv_g V_{act} S}{2L\lambda\Gamma} \ln\left(\frac{1}{R_2}\right) \ . \tag{2.27}$$

2.4 Steady-state power versus injection current

The output power has been derived as a function of injection current at equation (2.25). However, that equation only is valid when the injection current is larger than the threshold current. A more rigorous expression for the steady-state output power can be derived from the rate equations by considering the spontaneous emission contribution.By setting the time derivation in equations (2.1) and (2.2), the steady-state solution can be obtained by

$$\frac{I}{qV_{act}} - \frac{N}{\tau_c} + \frac{g_0(N - N_0)}{1 + \epsilon S} S = 0 \ , \tag{2.28}$$

$$\frac{\Gamma g_0(N - N_0)}{1 + \epsilon S} S - \frac{S}{\tau_p} + \frac{\Gamma \beta_{sp} N}{\tau_c} = 0 \ . \tag{2.29}$$

At threshold, the gain balances the losses, spontaneous emission term vanishes from the steady state photon equation (2.29), one obtains

$$\frac{\Gamma g_0(N_{th} - N_0)}{1 + \epsilon S} = \frac{1}{\tau_p} \ . \tag{2.30}$$

Since ϵS is quite small at threshold, it can be neglected in the above equation as

$$\Gamma g_0(N_{th} - N_0) = \frac{1}{\tau_p} \ , \tag{2.31}$$

therefore, the threshold carrier density is derived as

$$N_{th} = N_0 + \frac{1}{\Gamma g_0 \tau_p} \ . \tag{2.32}$$

At threshold, the photon density is small and can be neglected, equation (2.28) can be rewritten as

$$\frac{I_{th}}{qV_{act}} - \frac{N_{th}}{\tau_c} = 0 \ . \tag{2.33}$$

The threshold current can be obtained by rearranging the above equation and substituting equation (2.32),

$$I_{th} = \frac{qV_{act}}{\tau_c} N_{th} = \frac{qV_{act}}{\tau_c} \left(N_0 + \frac{1}{\Gamma g_0 \tau_p} \right) \ . \tag{2.34}$$

By substituting steady state photon equation (2.29) into the steady state carrier equation (2.28) and rearrange, yield:

$$S = \frac{\Gamma I \tau_p}{qV_{act}} - \frac{\tau_p}{\tau_c}(1 - \beta_{sp})\Gamma N \ , \tag{2.35}$$

then rearrange (2.28) and solve for the carrier density N as:

$$N = \frac{\Gamma g_0 N_0 + \frac{1}{\tau_p}}{\Gamma g_0 + \frac{\Gamma \beta_{sp}}{\tau_c} \frac{1+\epsilon S}{S}} = \frac{N_{th}}{1 + \frac{\beta_{sp}}{g_0 \tau_c} \frac{1+\epsilon S}{S}} \ . \tag{2.36}$$

By Substituting the above equation in (2.35),yield:

$$S = \frac{\Gamma I \tau_p}{qV_{act}} - \frac{\tau_p}{\tau_c}(1 - \beta_{sp})\Gamma \frac{N_{th}}{1 + \frac{\beta_{sp}}{g_0 \tau_c} \frac{1+\epsilon S}{S}} \tag{2.37}$$

then substitute (2.34) into the above equation and rearrange it as following:

$$\frac{qV_{act}\beta_{sp}}{g_0\tau_c\tau_p\Gamma}+\frac{qV_{act}}{\tau_p}\left(1+\frac{\beta_{sp}\epsilon}{g_0\tau_c}\right)\frac{S}{\Gamma}=\left(1+\frac{\epsilon\beta_{sp}}{g_0\tau_c}\right)I+\frac{\Gamma}{S}\frac{\beta_{sp}}{g_0\tau_c}I-(1-\beta_{sp})I_{th}\ . \quad (2.38)$$

By defining the leaky current as

$$I_S=\frac{qV_{act}\beta_{sp}}{g_0\tau_c\tau_p\Gamma}\ , \quad (2.39)$$

(2.38) can be rearranged as:

$$I_S+\left(1+\frac{\beta_{sp}\epsilon}{g_0\tau_c}\right)\frac{qV_{act}}{\tau_p}\frac{S}{\Gamma}=\left(1+\frac{\beta_{sp}\epsilon}{g_0\tau_c}\right)I+\frac{\Gamma}{\frac{qV_{act}}{\tau_p}S}I_SI-(1-\beta_{sp})I_{th}\ . \quad (2.40)$$

Because $\frac{\beta_{sp}\epsilon}{g_0\tau_c}\ll 1$ and $\beta_{sp}\ll 1$ the above equation can be simplified as

$$\left(\frac{qV_{act}}{\Gamma\tau_p}S\right)^2-(I-I_S-I_{th})\frac{qV_{act}}{\Gamma\tau_p}S-I_S\ I=0\ . \quad (2.41)$$

By substituting equation (2.24) into (2.41), the equation for output power is express as

$$\left(\frac{2q\lambda}{\eta hc}P\right)^2-(I-I_S-I_{th})\left(\frac{2q\lambda}{\eta hc}P\right)-I_S\ I=0 \quad (2.42)$$

and (2.42) can be simplified as

$$(FP)^2-(I-I_S-I_{th})FP-I_S\ I=0 \quad (2.43)$$

and

$$F=\frac{2q\lambda}{\eta hc} \quad (2.44)$$

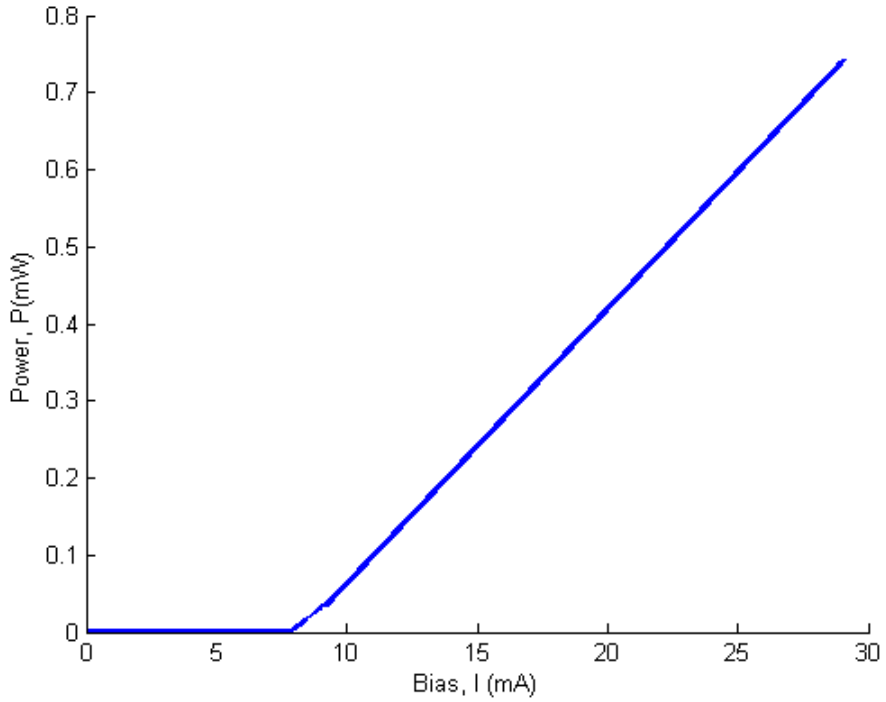

Figure 2.1: Optical power(mW) versus bias current(mA) characteristics

2.5 Turn-on delay

No laser diode that lase instantly when the injection current is applied. When a laser diode is biased with a certain current, the carriers are accumulated in the active region. The spontaneous emission dominates at this stage and the laser does not lase. When the carrier density reaches a certain level at which the population inversion happens, the stimulated emission dominates and the laser starts lasing. When the carrier density is further accumulated to a higher level , the photons are able to overcome the absorptions in the cavity and emitted from the facets. The interval

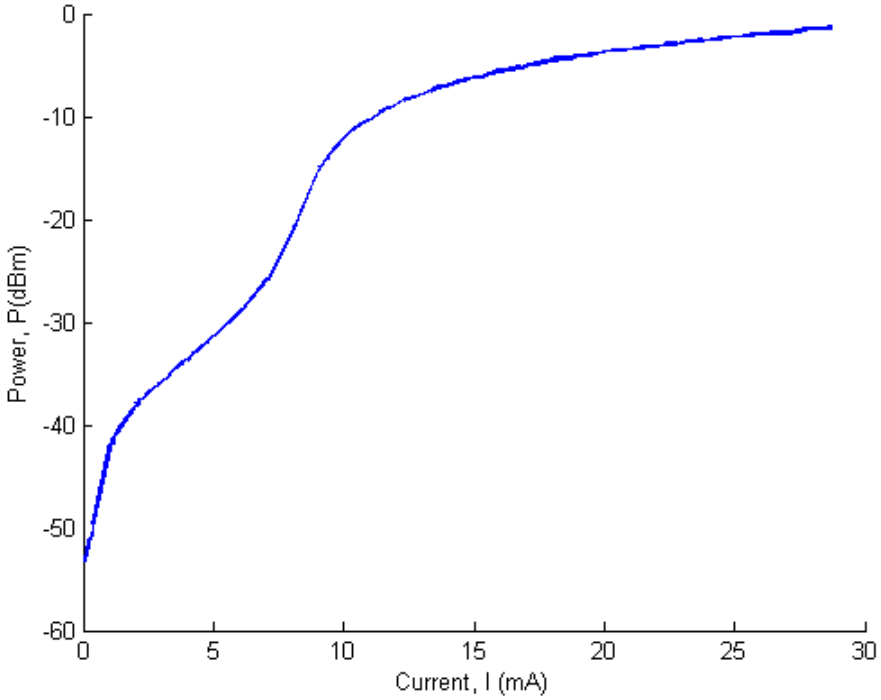

Figure 2.2: Optical power(dBm) versus bias current(mA) characteristics

from the injection current applied to the lasing power going out from the laser diode called turn-on delay.

The turn-on delay can be derived from the rate equation model.Before the threshold current is reached, the photon density is neglected. Equation (2.1) becomes

$$\frac{dN}{dt} = \frac{I}{qV_{act}} - \frac{N}{\tau_c} \ . \tag{2.45}$$

If the current is switched on at $t = 0$ with carrier density $N = N_{init}$, which is the initial carrier density, and turned on at $t = t_s$ with carrier density $N = N_{th}$, by

integrating over the carrier accumulated, the turn-on delay is

$$t_s = qV_{act} \int_{N_{init}}^{N_{th}} \left(I - qV_{act} \frac{N}{\tau_c} \right)^{-1} dN \ , \tag{2.46}$$

by replacing the carrier density with the injection current, the turn-on delay is described as:

$$t_s = \tau_c \ln \left(\frac{I - I_{init}}{I - I_{th}} \right) \tag{2.47}$$

Therefore, turn-on delay can be viewed as the time period of increasing current from the initial value I_{init} to value I that is greater than the threshold current I_{th} .

2.6 Small signal intensity modulation response

The intensity modulation response is one of the most important characteristics indicating how fast a laser diode can be modulated in the light-wave communication system[22]. When the modulation amplitude is small, the rate equations can be linearized and an analytical solution of the laser diode transfer function can be obtained. By setting the time derivations to zero in the rate equations (2.1) and (2.2), the steady-state solution can be obtained as

$$0 = \frac{I(t)}{qV_{act}} - \frac{N(t)}{\tau_c} - g_0 \frac{N(t) - N_0}{1 + \epsilon S(t)} S(t) \tag{2.48}$$

and

$$0 = \Gamma g_0 \frac{N(t) - N_0}{1 + \epsilon S(t)} S(t) - \frac{S(t)}{\tau_p} + \frac{\Gamma \beta_{sp} N(t)}{\tau_c} \ . \tag{2.49}$$

When the small modulation current is applied, the laser diode is working at the above threshold situation in which the spontaneous emission can be neglected. Therefore the photon density can be derived as:

$$S = \frac{\tau_p \Gamma}{qV_{act}}(I - I_{th}) \ . \tag{2.50}$$

Assume that the laser is biased above threshold with a current I_0 , resulting in a photon density S_0. A small signal modulation $\Delta I(t)$ is added to the bias current. The total injection current is

$$I(t) = I_0 + \Delta I(t) \ . \tag{2.51}$$

The photon density is expected to deviate from their steady states according to

$$S(t) = S_0 + \Delta S(t) \ . \tag{2.52}$$

The carrier density is expected to deviate from their steady states according to

$$N(t) = N_0 + \Delta N(t) \ . \tag{2.53}$$

To linearize the rate equations, the Taylor series expansion on the optical gain is performed around the biasing point as

$$g\left(N, S\right) = g\left(N_0, S_0\right) + \frac{\partial g}{\partial N}\Delta N + \frac{\partial g}{\partial S}\Delta S + ... \tag{2.54}$$

then, substitute (2.51), (2.51), (2.51) and (2.54) into rate equation (2.1) and (2.2):

$$\frac{d\Delta N}{dt} = \frac{\Delta I}{qV_{act}} - \left(\frac{1}{\tau_c} + \frac{\partial g}{\partial N}S_0\right)\Delta N - \left(g_0 + \frac{\partial g}{\partial S}S_0\right)\Delta S \tag{2.55}$$

and

$$\frac{d\Delta S}{dt} = \left(\Gamma g_0 + \Gamma\frac{\partial g}{\partial S}S_0 - \frac{1}{\tau_p}\right)\Delta S + \left(\Gamma\frac{\partial g}{\partial N}S_0 + \frac{\beta_{sp}}{\tau_c}\Gamma\right)\Delta N \ . \tag{2.56}$$

For a laser diode working at above threshold, the spontaneous emission and gain saturation can be neglected, which:

$$\Gamma g_0 - \frac{1}{\tau_p} = -\frac{\beta_{sp}N_0}{S_0\tau_c} \approx 0 \tag{2.57}$$

and

$$\Gamma\frac{\partial g}{\partial S}S_0 \approx 0 \ , \tag{2.58}$$

substitute the above approximations (2.57) and (2.57) into (2.56) and obtain

$$\frac{d\Delta S}{dt} = \left(\Gamma\frac{\partial g}{\partial N}S_0\right)\Delta N \ . \tag{2.59}$$

By substituting (2.57) into (2.55) to have:

$$\frac{d}{dt}\Delta N = \frac{\Delta I}{qV_{act}} - \left(\frac{1}{\tau_c} + \frac{\partial g}{\partial N}S_0\right)\Delta N - \frac{1}{\Gamma\tau_p}\Delta S \ . \tag{2.60}$$

The current driving the laser varies as sinusoidal function with angular frequency Ω and amplitude $\Delta\tilde{I}(\Omega)$, the variations of current, photon and carrier numbers can be written as

$$\Delta I(t) = \Re\left\{\Delta\tilde{I}(\Omega)\exp(j\Omega t)\right\} \ , \tag{2.61}$$

$$\Delta N(t) = \Re\left\{\Delta\tilde{N}(\Omega)\exp(j\Omega t)\right\} \tag{2.62}$$

and

$$\Delta S(t) = \Re\left\{\Delta\tilde{S}(\Omega)\exp(j\Omega t)\right\} \tag{2.63}$$

By substituting the above equations into (2.59), one gets

$$j\Omega\Delta\tilde{S} = \left(\Gamma\frac{\partial g}{\partial N}S_0\right)\Delta\tilde{N} \ . \tag{2.64}$$

Similarly, the carrier rate equation is given by

$$j\Omega\Delta\tilde{N} = \frac{\Delta\tilde{I}}{qV_{act}} - \left(\frac{1}{\tau_c} + \frac{\partial g}{\partial N}S_0\right)\Delta\tilde{N} - \frac{1}{\Gamma\tau_p}\Delta\tilde{S} \ . \tag{2.65}$$

Rearranging (2.64) and express $\Delta\tilde{N}$ as:

$$\Delta\tilde{N} = \frac{j\Omega\Delta\tilde{S}}{\Gamma\frac{\partial g}{\partial N}S_0}, \tag{2.66}$$

then, substitute $\Delta\tilde{N}$ expression into (2.65), one has

$$\frac{\Delta\tilde{I}}{qV_{act}} = \left[\left(\frac{1}{\tau_c} + \frac{\partial g}{\partial N}S_0 + j\Omega\right)\frac{j\Omega}{\frac{\Gamma\frac{\partial g}{\partial N}S_0}{\tau_p}\tau_p} + \frac{1}{\Gamma\tau_p}\right]\Delta\tilde{S} \ . \tag{2.67}$$

By defining the relaxation oscillation frequency

$$\Omega_R = \left(\frac{\frac{\partial g}{\partial N}S_0}{\tau_p}\right)^{1/2} = \left(\frac{\Gamma\frac{\partial g}{\partial N}(I - I_{th})}{qV_{act}}\right)^{1/2} = \left(\frac{\Gamma g_0(I - I_{th})}{qV_{act}}\right)^{1/2} \tag{2.68}$$

and the relaxation damping factor

$$\Gamma_R = \frac{1}{2}\left(\frac{1}{\tau_c} + \frac{\partial g}{\partial N}S_0\right) = \frac{1}{2}\left(\frac{1}{\tau_c} + \frac{g_0\Gamma\tau_p}{qV_{act}}\left(I - I_{th}\right)\right) = \frac{1}{2}\left(\frac{1}{\tau_c} + \tau_p{\Omega_R}^2\right) \tag{2.69}$$

equation (2.67) can be simplified to

$$\frac{\Delta\tilde{I}}{qV_{act}} = \left[\left(2\Gamma_R + j\Omega\right)\frac{j\Omega}{\Gamma\Omega_R^2\tau_p} + \frac{1}{\Gamma\tau_p}\right]\Delta\tilde{S}\ , \tag{2.70}$$

therefore, $\Delta\tilde{S}\left(\Omega\right)$ can be obtained easily from the above equation as

$$\Delta\tilde{S}\left(\Omega\right) = \frac{\frac{\Gamma\tau_p}{qV_{act}}\Omega_R^2}{2j\Gamma_R\Omega + \Omega_R^2 - \Omega^2}\Delta\tilde{I}\left(\Omega\right)\ . \tag{2.71}$$

By substituting $S\left(0\right) = \frac{\Gamma\tau_p}{qV_{act}}\left[I\left(0\right) - I_{th}\right]$,which from equation (2.50), into the above equation, a clear relationship between the input current and the output photons is derived as

$$\frac{\Delta\tilde{S}\left(\Omega\right)}{\tilde{S}\left(0\right)} = \frac{\Omega_R^2}{2j\Gamma_R\Omega + \Omega_R^2 - \Omega^2}\frac{\Delta\tilde{I}\left(\Omega\right)}{\tilde{I}\left(0\right)}\ . \tag{2.72}$$

The transfer function of this laser diode under the small signal modulation is obtained as

$$H(\Omega) = \frac{\Omega_R^2}{(\Omega_R^2 - \Omega^2) + 2j\Gamma_R\Omega} \tag{2.73}$$

and the magnitude of this transfer function can be express as:

$$\left|H\left(\Omega\right)\right| = \frac{\Omega_R^2}{\sqrt{\left(2\Gamma_R\Omega\right)^2 + \left(\Omega_R^2 - \Omega^2\right)^2}}\ . \tag{2.74}$$

The output power response is expressed as

$$\Delta P(f) = \frac{V\eta hc}{2\Gamma\tau_p\lambda}\Delta S = \frac{V\eta hc}{2\Gamma\tau_p\lambda}H(f)\left(\frac{\Gamma\tau_p}{qV}\right)\Delta I = \frac{\eta hc\Delta I}{2q\lambda}H(f)\ . \tag{2.75}$$

The simulation results of the small signal intensity modulation responses of a DFB

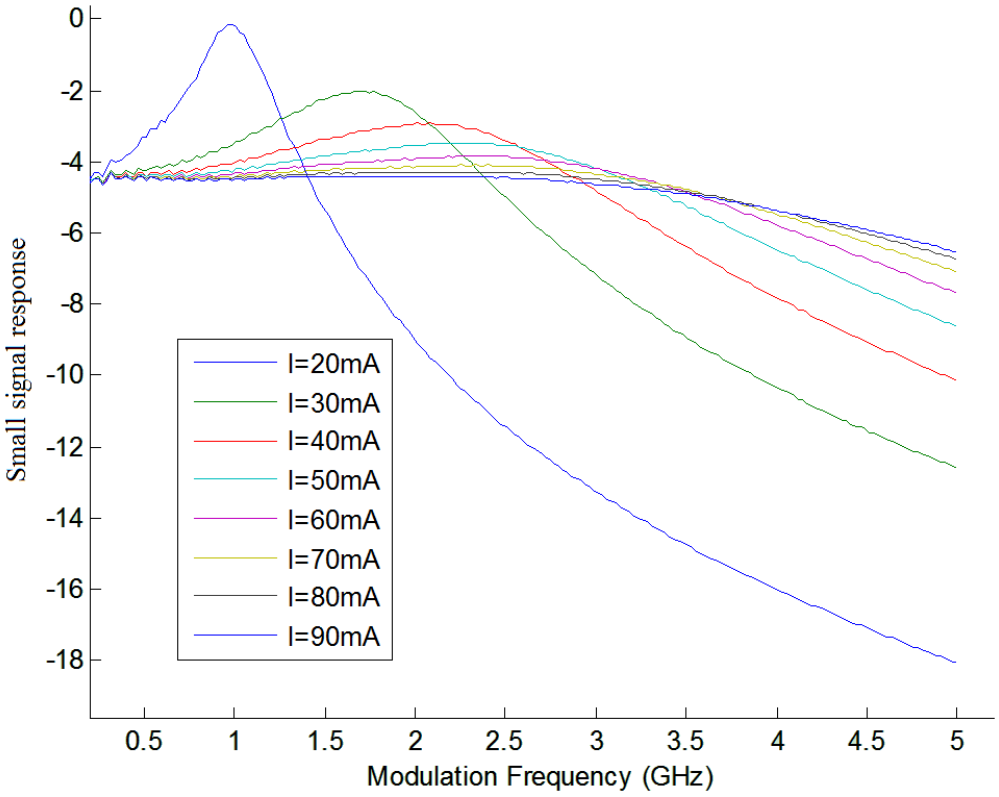

Figure 2.3: Small signal intensity modulation responses of a DFB laser at different biased currents.

laser at different biased currents are given in Figure 2.3. The relaxation oscillation frequency is located at the peak of the response curve. It shows that with the increase of biased current, the relaxation oscillation frequency shifts to higher level. The

relative response can be obtained by subtract the response at a lower biased current from the ones biased at higher biased currents[23][24].

The relative intensity modulation response is given by

$$\Delta H(f) = 10 \log \left| \frac{H(\Omega, \Omega_R, \Gamma_R)}{H(\Omega, \Omega_{R0}, \Gamma_{R0})} \right| . \tag{2.76}$$

The small signal intensity modulation responses of a DFB laser relative to the response of 20mA biased current is shown in Figure 2.4

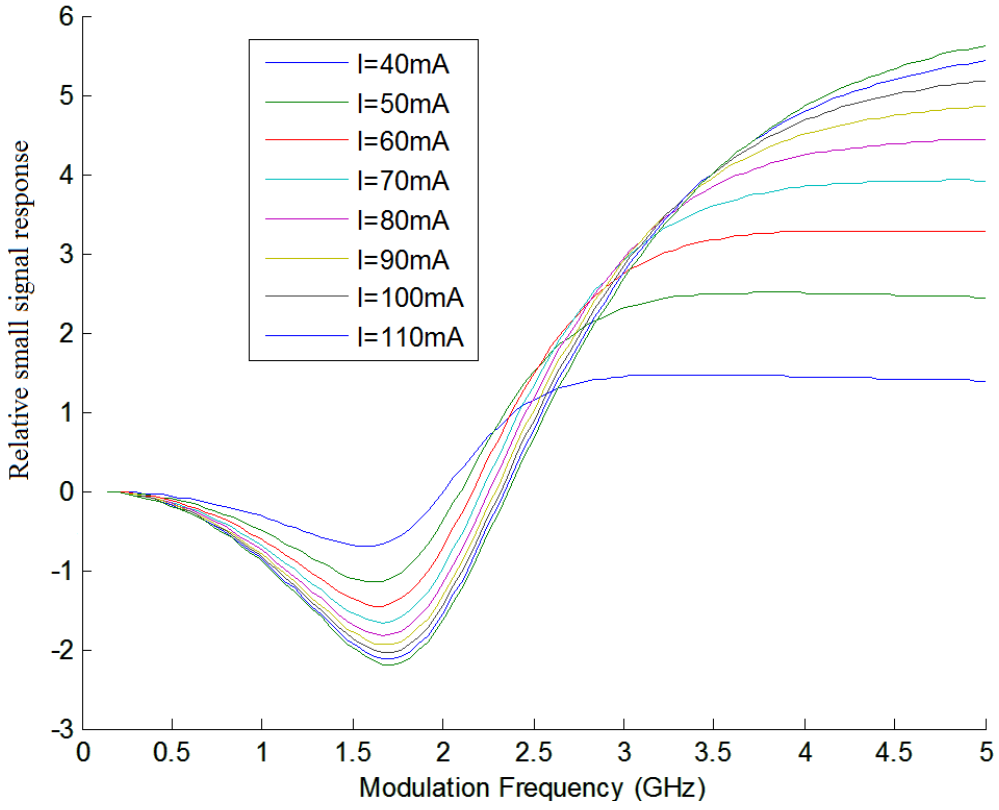

Figure 2.4: Small signal intensity modulation responses of a DFB laser at different biased currents relative to $20mA$ bias current.

2.7 Small signal response through dispersive optical fiber

The light-wave signal generated by a DFB laser is not purely monochromatic. The spectrum of the output signal is located at a central frequency and has a certain line-width from several kilo-Hz to a couple of mega-Hz. While the DFB laser is directly modulated with injection current, the central frequency of the light-wave changes with the output power. This is called frequency chirping. The frequency chirping property causes the line-width of the light-wave even larger when the laser diode is modulated. When passing the chirped light-wave through a dispersive optical fiber, the carried signal is distorted and the output power through the optical fiber is affected. The small signal intensity modulation response is important to study the performance of a laser diode in an optical fiber system.

The input signal to the optical fiber is directly modulated laser diode with intensity modulation characteristic as:

$$\Delta S_{in}(j\omega) = \left(\frac{\tau_p}{q}\right) H(j\omega)\,\Delta I(j\omega) \ , \tag{2.77}$$

where

$$H(j\omega) = \frac{\omega_R^2}{(j\omega)^2 + 2j\Gamma_R\omega + \omega_R^2} \ . \tag{2.78}$$

The intensity modulation at the output of fiber is given by

$$\Delta S_{out}(j\omega) = \left[\cos\left(F_D\omega^2\right) - \alpha\left(1 - j\frac{\omega_c}{\omega}\right)\sin\left(F_D\omega^2\right)\right] \cdot \left(\frac{\tau_p}{q}\right) H(j\omega)\,\Delta I(j\omega) \ , \tag{2.79}$$

where the optical fiber transfer function is given by

$$\begin{aligned} H_{fiber,dB} &= \Delta P_{fiber,dB} - \Delta P_{LD,dBm} \\ &= 10 \times \log \left[\cos\left(F_D \omega^2\right) - \alpha \left(1 - j\frac{\omega_c}{\omega}\right) \sin\left(F_D \omega^2\right) \right] \ . \end{aligned} \tag{2.80}$$

The parameters are

$$F_{\mathrm{D}} = \frac{\lambda^2 D L_{fibre}}{4\pi c} \tag{2.81}$$

and

$$\omega_c = \frac{\varepsilon \Gamma}{eV} \left(I - I_{th}\right) \ , \tag{2.82}$$

with D is the dispersion coefficient and L_{fiber} is the length of the fiber.

The simulation results of the transfer function of an optical fiber are shown in Figure 2.5.

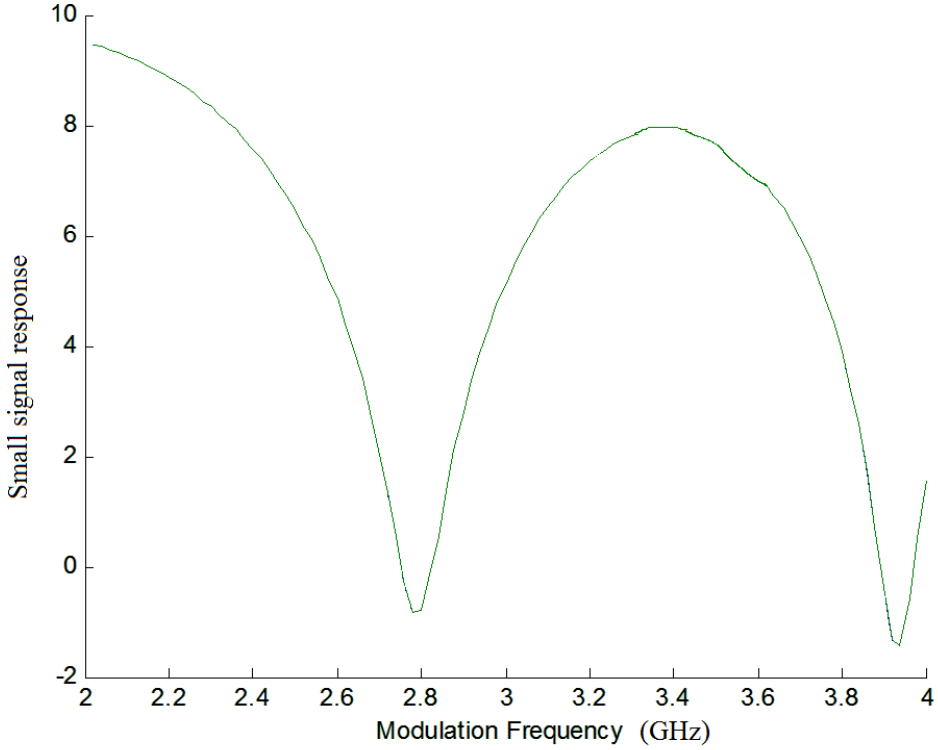

Figure 2.5: Small signal intensity modulation responses of a DFB laser through dispersive optical fiber at different biased currents

Chapter 3

Parameter Extraction Methods and Experiments

In this chapter, three parameter extraction experiments and the theory behind them will be introduced. In section 3.1, the measurement of steady-state optical power versus injection current is introduced and extraction experiment is also performed. In section 3.2, the measurement of small signal intensive modulation response is introduced and extraction experiment is also performed. In section 3.3,the measurement of small signal intensive modulation response through dispersive fiber is introduced and extraction experiment is also performed. The turn-on delay is a candidate of parameter extraction method that was introduced in section 2.5, however, this method is not every practically to perform in actual experiment. So turn-on delay measurement will not be used and not performed here. Section 3.4 shows the statistics of the experimental data. Finally in section 3.5 convert the experimental data to the actual parameters.

3.1 The steady-state power versus injection current measurement

In section 2.4, the steady-state laser output power versus its injection current relationship has been established, as shown in equation (2.43). By solve equation (2.43) and express output power in dBm, the following equation will be used in extraction of parameters

$$P_{dBm} = 10\log\left(\frac{I - I_{th} - I_S + \sqrt{(I - I_{th} - I_S)^2 + 4I_S\ I}}{2F}/1mW\right) \tag{3.1}$$

with three defined parameters as:

$$I_{th} = \frac{qV_{act}}{\tau_c}N_{th} = \frac{qV_{act}}{\tau_c}\left(N_0 + \frac{1}{\Gamma g_0 \tau_p}\right)\ , \tag{3.2}$$

$$I_S = \frac{qV_{act}\beta_{sp}}{g_0\tau_c\tau_p\Gamma}\ , \tag{3.3}$$

$$F = \frac{2q\lambda}{\eta hc}\ . \tag{3.4}$$

The reason that power is expressed in dBm is to make the data easy to analyze, as the power reading from the following setup are in dBm.

Experimental setup and result

This experimental is setup as the following: semiconductor laser is powered by power supply ILXLightwave LDC-3900 modular laser diode controller and the optical power is measured through Anritsu MT9810 Optical Test Set with Modula MU931421A Optical Sensor. Semiconductor lasers are mounted on THORLABS

LM9LP mount, then connect to the power supply. Both power supply and optical power sensors are communicated through GPIB ports to the controlling PC, and an automation software have been developed to control the instruments and analysis the result. The setup schematic is show in Figure 3.1:

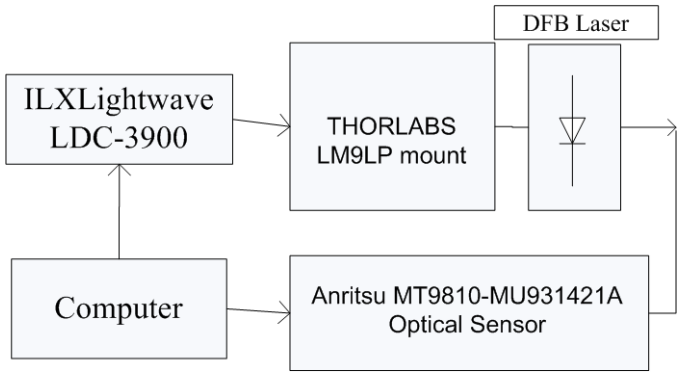

Figure 3.1: The schematic of Steady-State Optical power versus Injection current experiment.

Each semiconductor laser is test for 10 times with the same setup, and result of this individual laser is then averaged. The curve fitting process is utilize the least square error fitting method and one result of FU-650SDF-FW41M15 (made by Mitsubishi) single mode $1550nm$ DFB laser is shown as Figure 3.2 and Figure 3.3 with power in mW and dBm respectively:

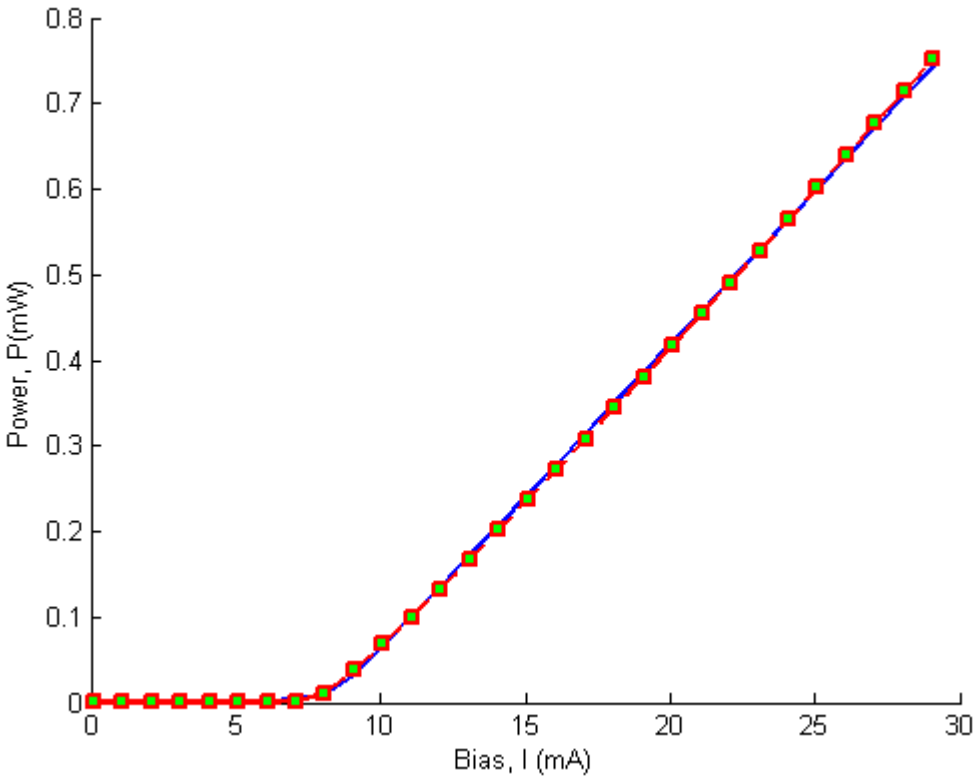

Figure 3.2: Steady state measurements of semiconductor laser (FU-650SDF-FW41M15) power (in mW) versus bias current (in mA), where the square representing the experimental data and line representing the line of best fit.

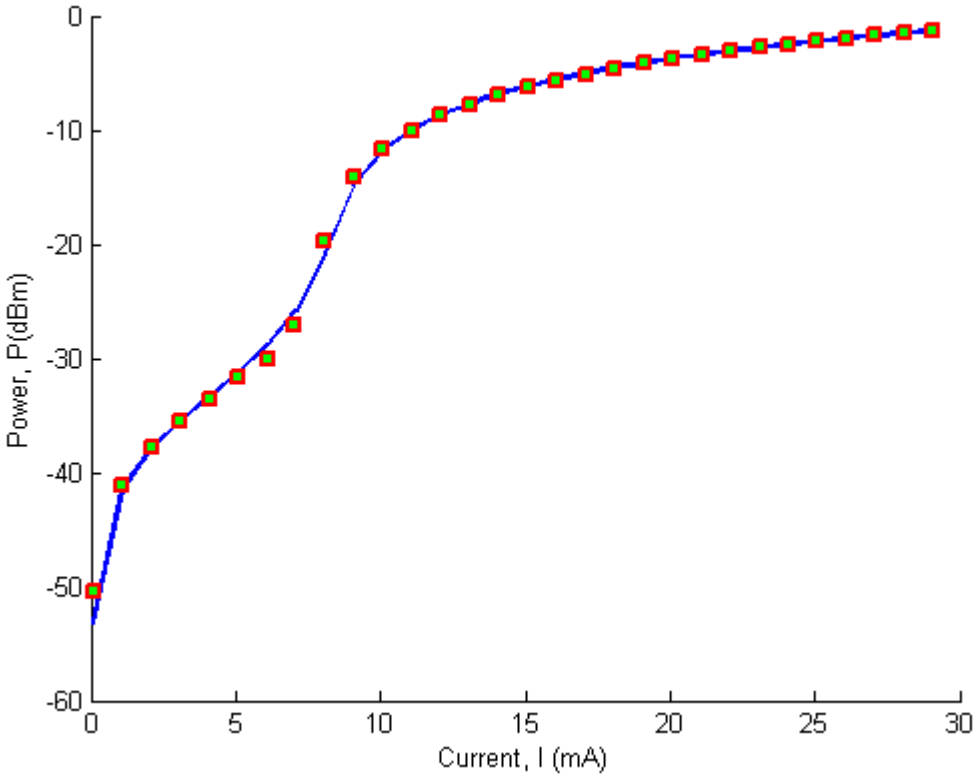

Figure 3.3: Steady state measurements of semiconductor laser (FU-650SDF-FW41M15) power (in dBm) versus bias current (in mA), where the square representing the experimental data and line representing the line of best fit.

For this particular laser FU-650SDF-FW41M15-J11808, the steady-state power versus injection current measurement has been performed for 10 times and the resulting curve has been curve fitted, the table 3.1 shows the experimental results and their averages.

The table above shows that the results from individual trails are fluctuated; that is the reason of performing same experiment for 10 times, averaging of the experimental result will help reduce the error between different trail and granting more accurate parameters for this particular experiment.

3.2 Small signal intensity modulation response measurement

As of section 2.6, the transfer function of this laser diode under the small signal modulation is obtained as[25]

$$H(\Omega) = \frac{\Omega_R^2}{(\Omega_R^2 - \Omega^2) + 2j\Gamma_R\Omega} \tag{3.5}$$

and the magnitude of this transfer function can be express as:

$$|H(\Omega)| = \frac{\Omega_R^2}{\sqrt{(2\Gamma_R\Omega)^2 + (\Omega_R^2 - \Omega^2)^2}} \ . \tag{3.6}$$

The output power response is expressed as

$$\Delta P(f) = \frac{V\eta hc}{2\Gamma\tau_p\lambda}\Delta S = \frac{V\eta hc}{2\Gamma\tau_p\lambda}H(f)\left(\frac{\Gamma\tau_p}{qV}\right)\Delta I = \frac{\eta hc\Delta I}{2q\lambda}H(f) \ . \tag{3.7}$$

Table 3.1: Experimental result of steady-state power versus injection current.

	$F(J/s)$	$I_{th}(mA)$	$I_S(\mu A)$
1	19.6860	9.76	13.5
2	19.9725	9.6	12.6
3	19.9725	9.68	10.8
4	19.686	9.6	11.7
5	20.259	9.68	12.6
6	19.686	9.76	11.7
7	20.259	9.6	12.6
8	19.686	9.6	10.8
9	19.686	9.68	12.6
10	19.3995	9.76	10.8
Average	19.82925	9.672	11.9709

The simulation results of the small signal intensity modulation responses of a DFB laser at different biased currents are given in Figure 2.3. The relaxation oscillation frequency is located at the peak of the response curve. It shows that with the increase of biased current, the relaxation oscillation frequency shifts to higher level. The relative response can be obtained by subtract the response at a lower biased current from the ones biased at higher biased currents.

The relative intensity modulation response is given by

$$\Delta H\left(f\right) = 10\log\left|\frac{H\left(\Omega,\Omega_R,\Gamma_R\right)}{H\left(\Omega,\Omega_{R0},\Gamma_{R0}\right)}\right| \ . \tag{3.8}$$

The introduction of this relative intensity modulation response techniqueis important that it almost eliminates any limitations that could arise from the mounting fixture and the packaging of the laser, in addition to relaxing the requirements for accurate calibration of the experimental setup.[26][27]

Experimental setup and result

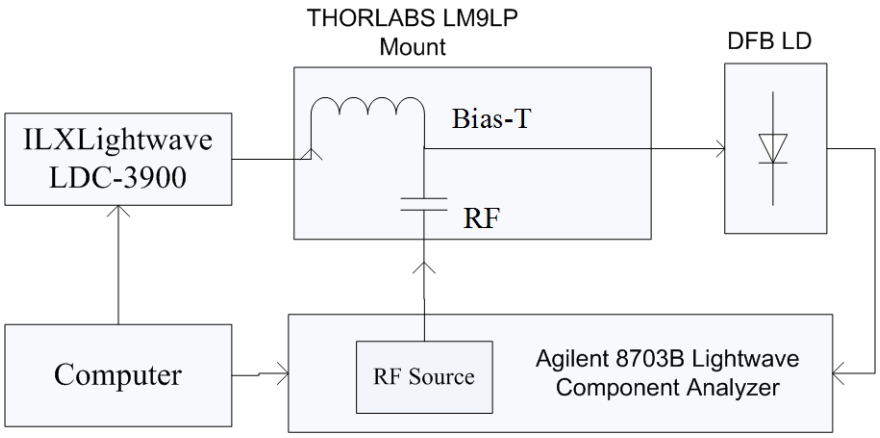

Figure 3.4: The schematic of small signal intensity modulation response experiment.

This experimental is setup as the following: semiconductor laser is powered by power supply ILXLightwave LDC-3900 modular laser diode controller and the small signal intensity modulation response is measured through Agilent 8703B Lightwave Component Analyzer. The current of the laser diode is directly modulated by an RF signal. The light-wave component analyzer modulate and sweep the frequency of all available bandwidth of the analyzer to the laser and measure the output power at each frequency in order to plot the small signal intensity modulation response with repeat at several bias currents. The Semiconductor lasers are mounted on THORLABS LM9LP mount and connect with the modulation signal from the Agilent 873B Lightwave Component Analyzer, and the THORLABS LM9LP mount also connect to the power supply. Both power supply and lightwave component analyzer are communicated through GPIB ports to the controlling PC, and an automation software

have been developed to control the instruments and analysis the result. The collected data are in the form of different response curve at different bias curve. And as the discussion of section 3.2, the relative intensity modulation technique is applied. Therefore, the collected data curve from the instrument will be processed to generate a relative power curve: the original data subtract the minimum biased current data to yield the relative curve.

The experimental result of small signal intensity modulation response curve on one of the FU-650SDF-FW41M15 under different bias currents is shown in Figure 3.5

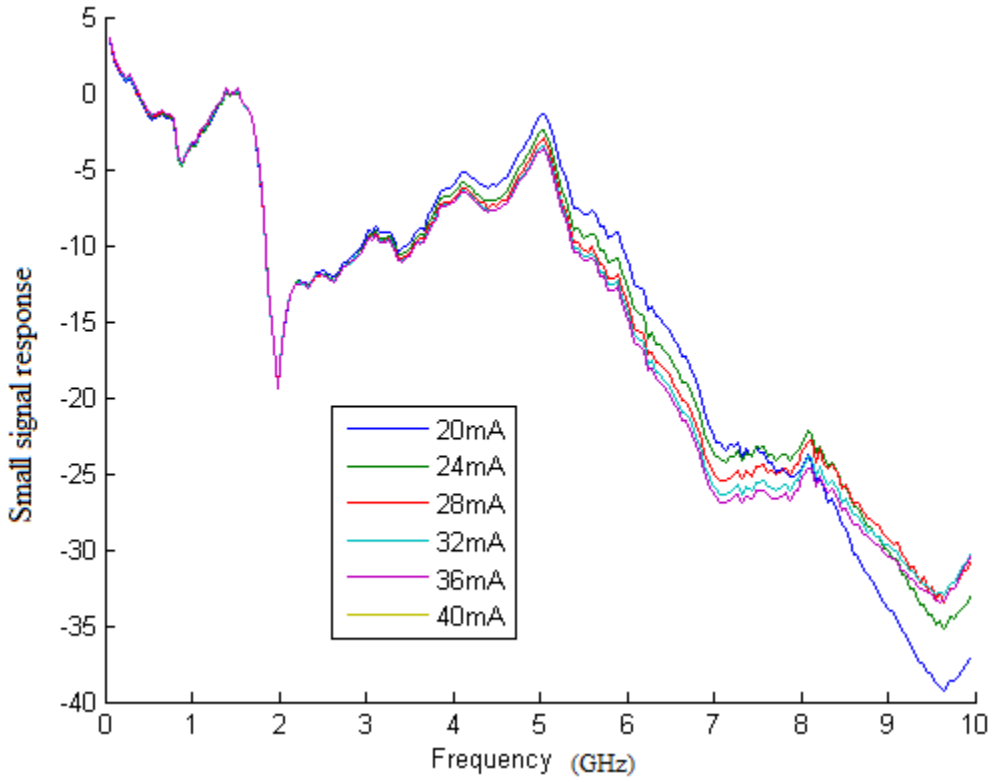

Figure 3.5: The experimental result of small signal IM response curve under different bias current with FU-650SDF-FW41M15 semiconductor DFB laser.

As it can be seen that this curve is close to the simulation result in terms of its shape, however, going under a lot of distortions.

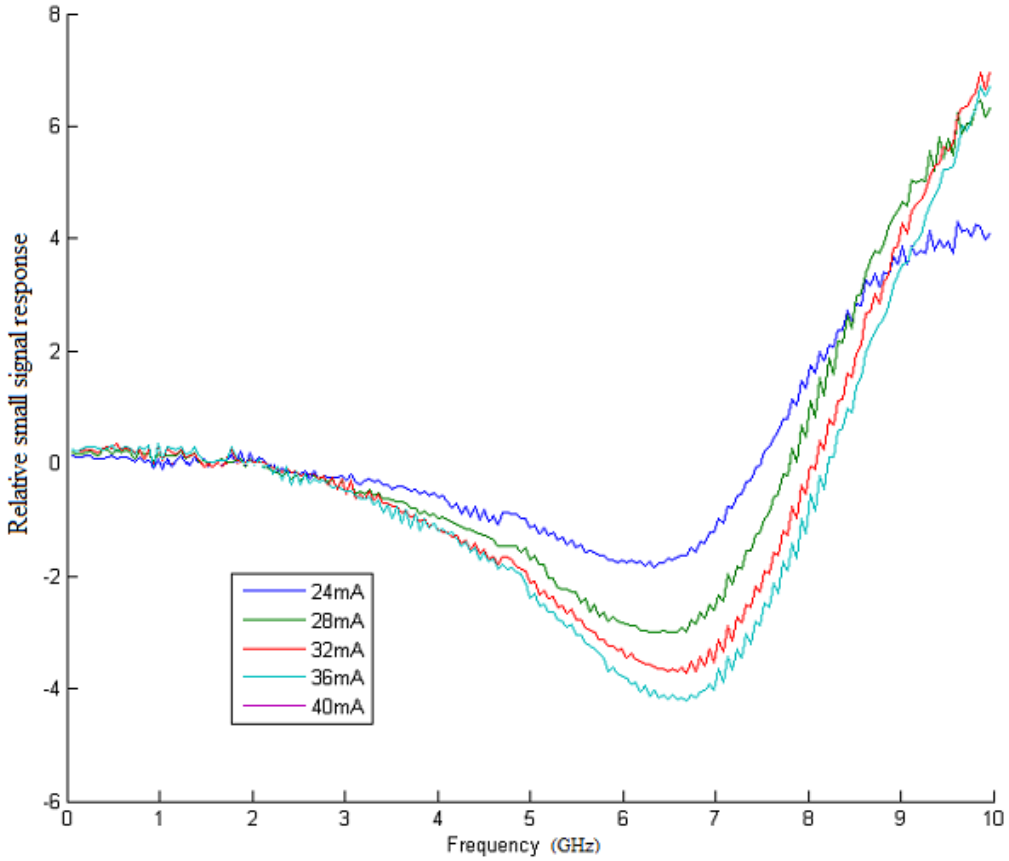

Figure 3.6: The experimental result of relative small signal IM response curve under different bias current with FU-650SDF-FW41M15 semiconductor DFB laser.

As discussed earlier in this section, these are due to the limitations that arise from the mounting fixture and the packaging of the laser. Therefore, the further process of the data require the relative intensity modulation response, which in my experiment that subtract all curve in Figure 3.5 with a base response curve, that has been picked as the $20mA$ response curve, and yield the following relative intensity modulation response curve in Figure 3.6

In particular, we are interested in the 1st curve that can be used to fit the parameters Ω_R, Γ_R, Ω_{R_0} and Γ_{R0} , where Ω_R and Ω_{R_0} corresponding to the relaxation oscillation frequency of the laser under $24mA$ and $20mA$ bias current respectively; Γ_R,Γ_{R0} corresponding to the damping factor of the laser under $24mA$ and $20mA$ bias current respectively. This particular interested curve is re-plotted as in Figure 3.7. And Figure 3.7 will be used in a fitting software that utilizes the least square error fitting method and the fitting curve is shown as in Figure 3.8

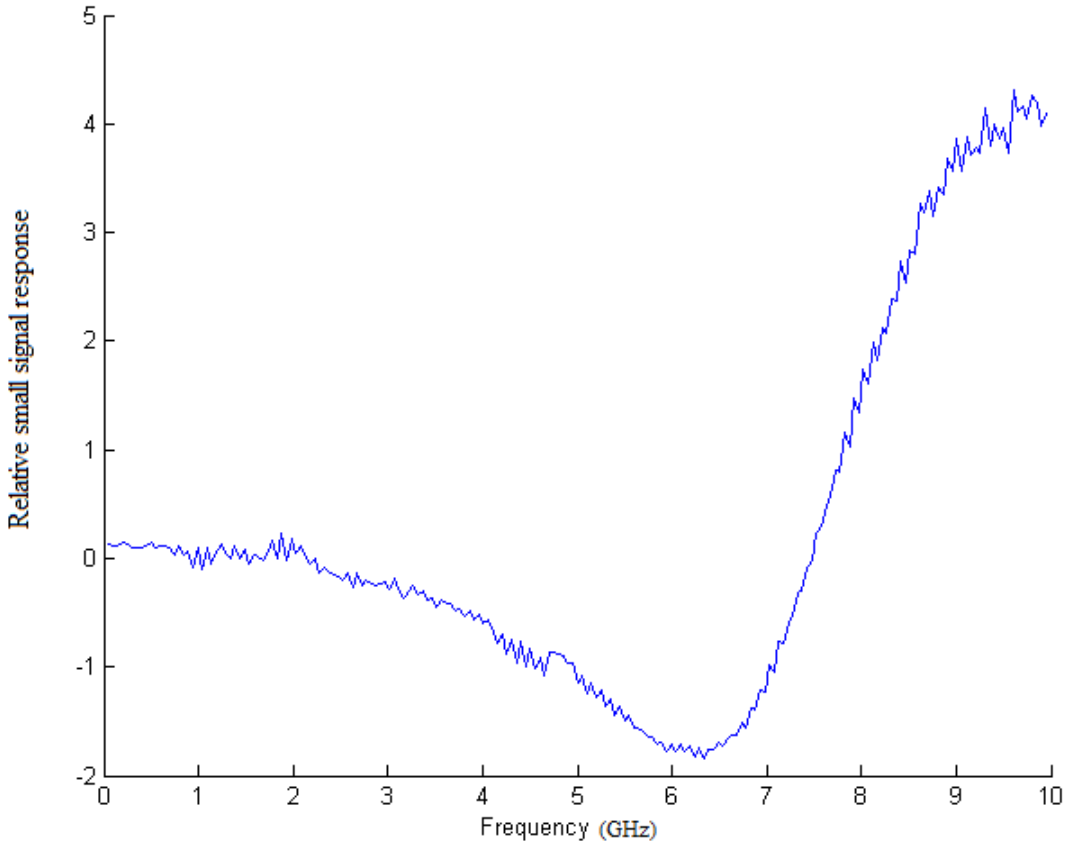

Figure 3.7: The experimental result of relative small signal IM response curve under 24mA bias current with FU-650SDF-FW41M15 semiconductor DFB laser.

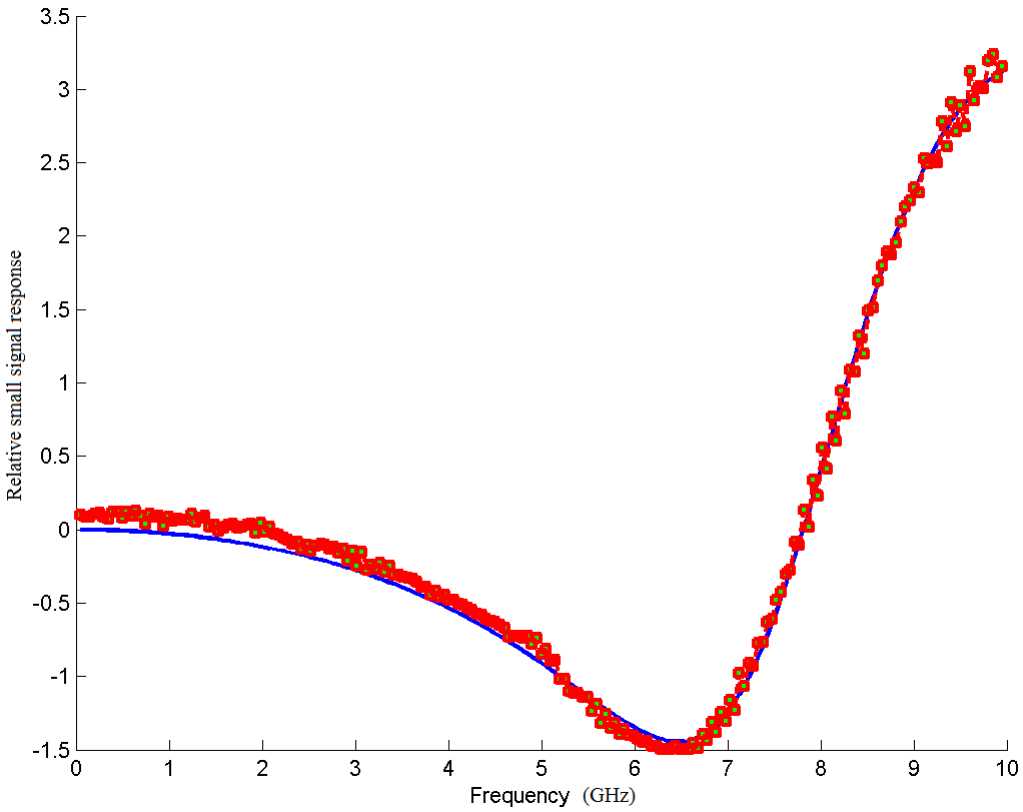

Figure 3.8: Curve fitting of experimental result of relative small signal IM response curve under 24mA bias current with FU-650SDF-FW41M15 semiconductor DFB laser.

Note: the the actual experiment, the result of frequencies are all measured in Hz rather than rad/s

For this particular laser FU-650SDF-FW41M15-J11808, the Small Signal Intensity Modulation Response Measurement has been performed for 10 times and the resulted curve has been curve fitted, table 3.2 shows the experimental results and their averages

Similar to the steady-state power versus injection current experiment, the results from individual trails are fluctuated, that is the reason of performing same experiment

Table 3.2: Experimental result of small signal intensity modulation response.

	$f_{R0}(GHz)$	$\gamma_{R0}(GHz)$	$f_R(GHz)$	$\gamma_R(GHz)$
1	7.3153315	9.38	9.195	12.39
2	7.3153315	9.14	9.11	12.32
3	7.3153315	9.26	9.195	12.46
4	7.3153315	9.14	9.195	12.425
5	7.3153315	9.38	9.11	12.11
6	7.3153315	9.34	9.195	12.495
7	7.3153315	9.38	9.195	12.425
8	7.3153315	9.14	9.11	11.9
9	7.3153315	9.14	9.11	12.04
10	7.3153315	9.18	9.11	12.75
Average	7.3153315	9.24	9.1525	12.264

for 10 times, averaging of the experimental result will help reduce the error between different trail and granting more accurate parameters for this particular experiment.

3.3 Measurement of small signal response through dispersive optical fiber

In section 2.7, the small signal response of semiconductor laser through dispersive optical fiber is studied with the following relationship that can be used to extract parameters

$$\begin{aligned} H_{fiber,dB} &= \Delta P_{fiber,dB} - \Delta P_{LD,dBm} \\ &= 10 \times \log\left[\cos\left(F_D\omega^2\right) - \alpha\left(1 - j\frac{\omega_c}{\omega}\right)\sin\left(F_D\omega^2\right)\right] \end{aligned} \tag{3.9}$$

with parameters

$$F_{\mathrm{D}} = \frac{\lambda^2 D L_{fibre}}{4\pi c} \tag{3.10}$$

and

$$\omega_c = \frac{\varepsilon\Gamma}{eV}\left(I - I_{th}\right) \tag{3.11}$$

where D is the fiber chromatic dispersion and L_{fiber} is the length of the fiber[28].

Experimental setup and result

This experimental is setup as the following: semiconductor laser is powered by power supply ILXLightwave LDC-3900 modular laser diode controller and the small signal intensity modulation response is measured through Agilent 8703B Lightwave Component Analyzer. The current of the laser diode is directly modulated by an RF signal. The light-wave component analyzer modulate and sweep the frequency of all available bandwidth of the analyzer to the laser and measure the output power at each frequency in order to plot the small signal intensity modulation response with repeat at several bias currents. The Semiconductor lasers are mounted on THORLABS LM9LP mount and connect with the modulation signal from the Agilent 873B Lightwave Component Analyzer, and the THORLABS LM9LP mount also connect to the power supply. Both power supply and lightwave component analyzer are communicated through GPIB ports to the controlling PC, and an automation software have been developed to control the instruments and analysis the result. The collected data are in the form of different response curve at different bias curve.

Due to equation (3.9), the experiment consists of two parts: In part one, with no long fiber conditions that small signal IM response curve is measured directly. In part

two, an extra SMF-28 fiber with length of 25.3 km is connected to the laser before it attach to the optical component analyzer. The schematic of part one is the same as the Small signal Intensity Modulation from last section as show in Figure 3.4. The part two schematic is shown in Figure 3.9

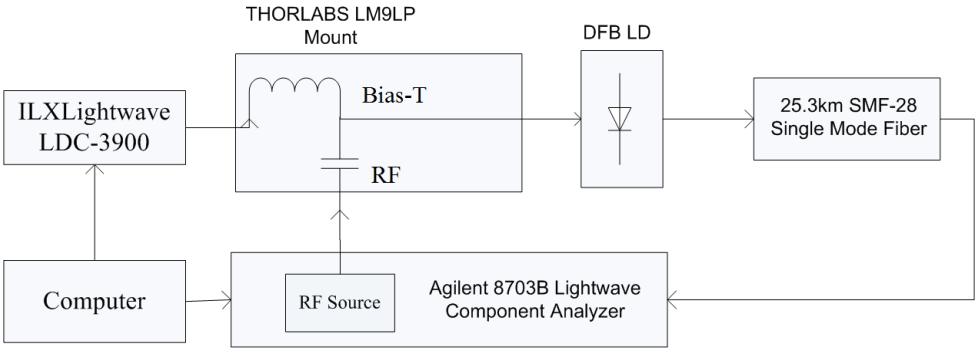

Figure 3.9: The schematic of small signal intensity modulation response through dispersive fiber experiment.

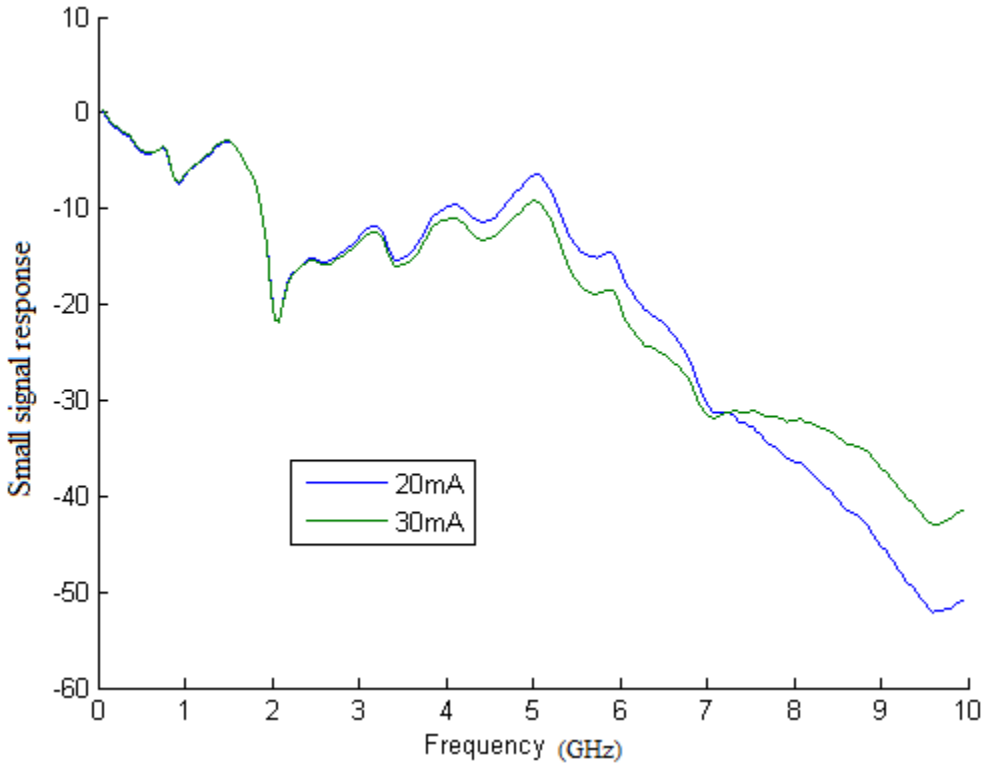

Figure 3.10: The part one of small signal IM response through dispersive fiber at two different bias current.

The result of part one for one of DFB laser FU-650SDF-FW41M15 is shown as in Figure 3.10

The result of part two for the same laser is shown in Figure 3.11

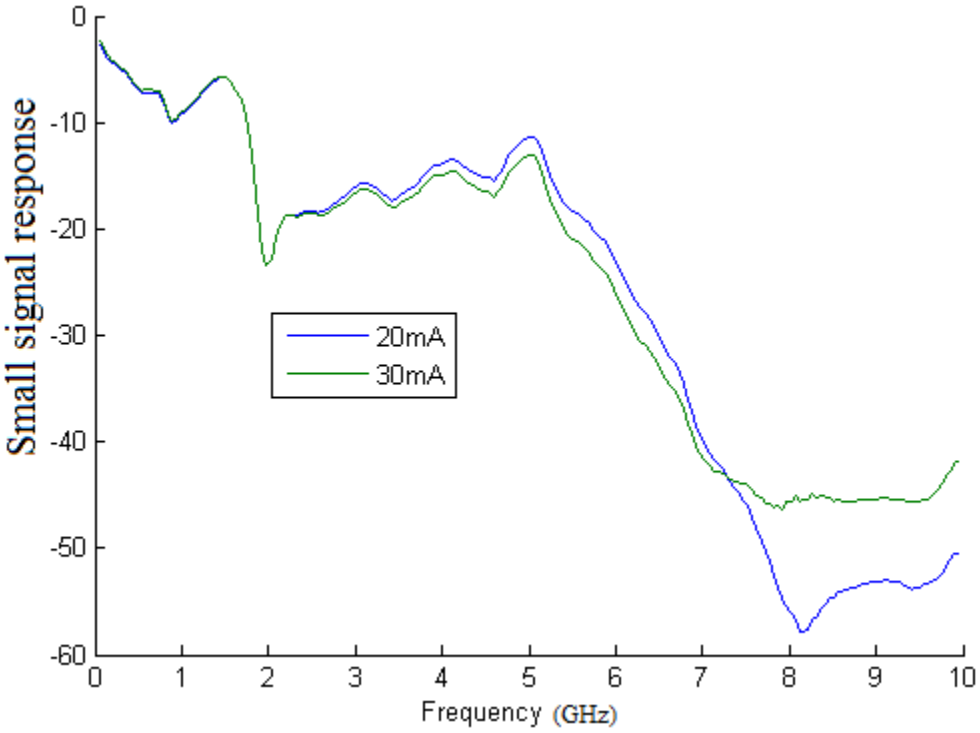

Figure 3.11: The part two of small signal IM response through dispersive fiber at two different bias current.

In term of processing of the data, the difference of the curve from the above figures (Figure 3.10 and Figure 3.11) are plotted, Note that due to the extra piece of fiber are attached, there are expected loss of the fiber and the extra connectors loss. The connector loss are around $1dBm$ loss per connector. To compensate for this loss and making the following fitting process easy, the curve will be bring up to start at zero dB, as the equation (3.9) equals to zero at low frequency and increase slowly at the low frequency. The difference curve is shown as in Figure 3.12

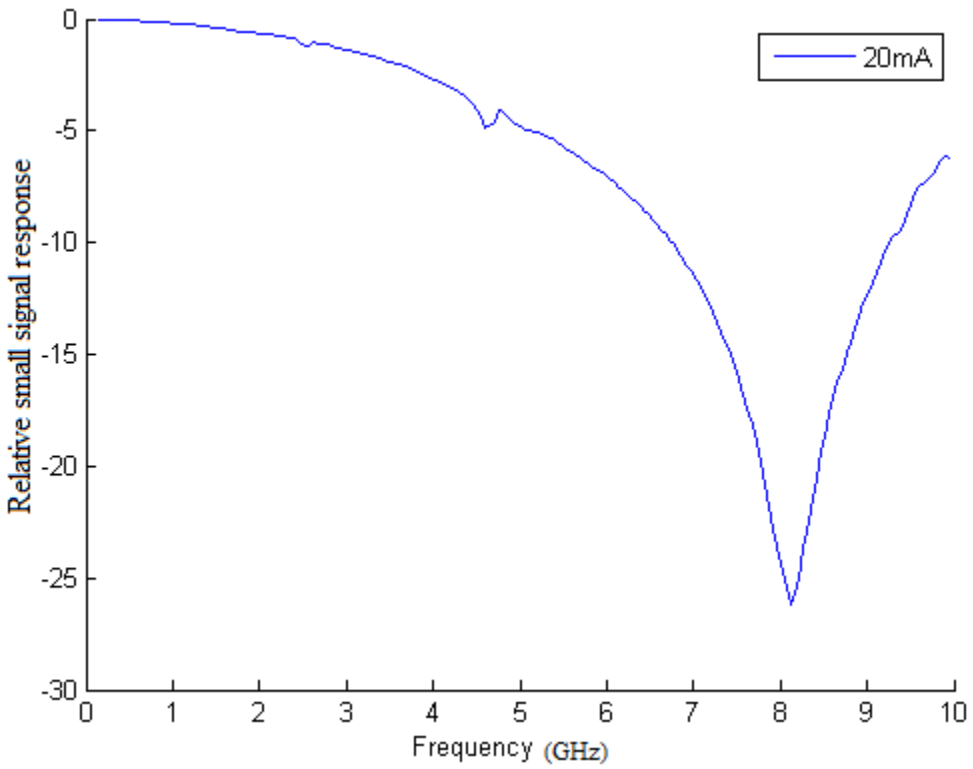

Figure 3.12: The small signal IM response through dispersive fiber difference curve at bias current of 20mA.

Finally, the Figure 3.12 is fitted through least square error fitting method, and the fitted curve is shown in Figure 3.13

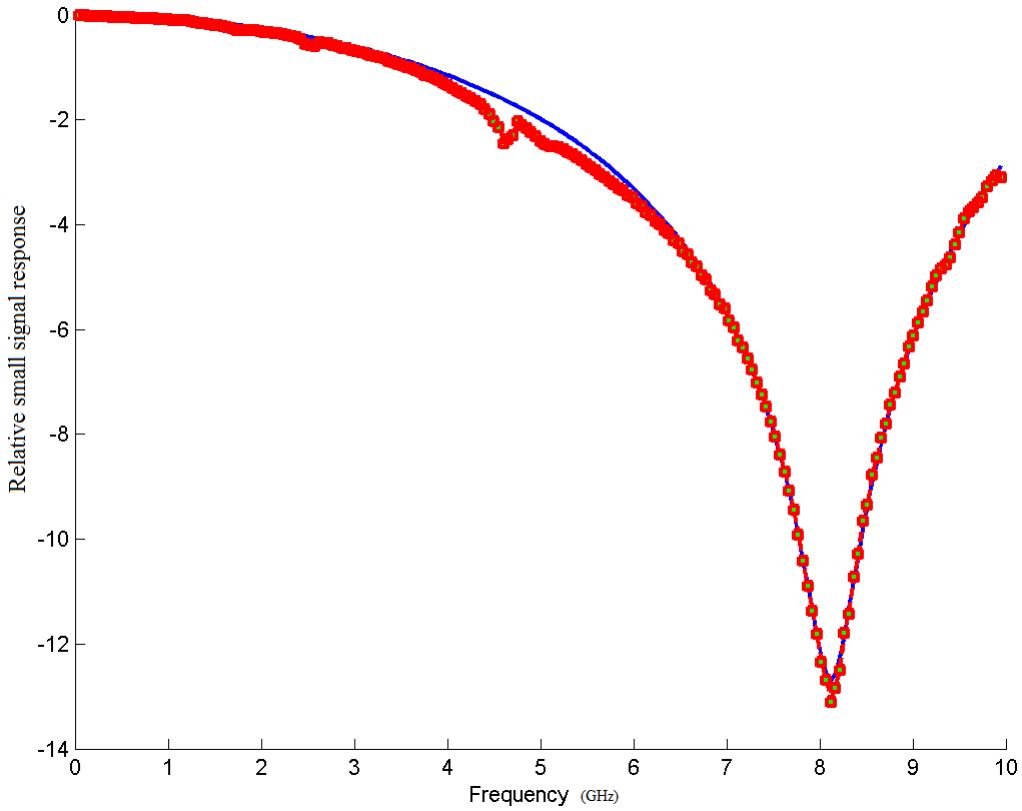

Figure 3.13: Curve fitting of small signal IM response through dispersive fiber difference curve at bias current of 20mA.

For this particular laser FU-650SDF-FW41M15-J11808, the Small Signal Response through Dispersive Optical Fiber measurement has been performed for 10 times and the resulting curve has been curve fitted, table 3.3 shows the experimental results and their averages.

As from the table above that the results from individual trails are fluctuated, that is the reason of performing same experiment for 10 times, averaging of the experimental result will help reduce the error between different trail and granting more accurate parameters for this particular experiment.

Table 3.3: Experimental result of small signal intensity modulation response through dispersive fiber.

	α	$f_c(GHz)$	$F_D(1 \times 10^{-22} Hz)$
1	2.34	0.475	1.55
2	2.44	0.475	1.50
3	2.36	0.51	1.55
4	2.4	0.51	1.53
5	2.4	0.51	1.53
6	2.4	0.51	1.53
7	2.4	0.51	1.53
8	2.4	0.51	1.53
9	2.4	0.51	1.53
10	2.36	0.545	1.55
Average	2.39	0.5065	1.53

3.4 Statistics of Experimental Data

There are totally 20 samples of semiconductor DFB lasers tested under experiment. They are all of the same model (FU-650SDF-FW41M15) and purchased together from the manufacture, Mitsubishi.

Each sample has been tested under the same conditions for 10 times and the average has been take into account in the following analysis.

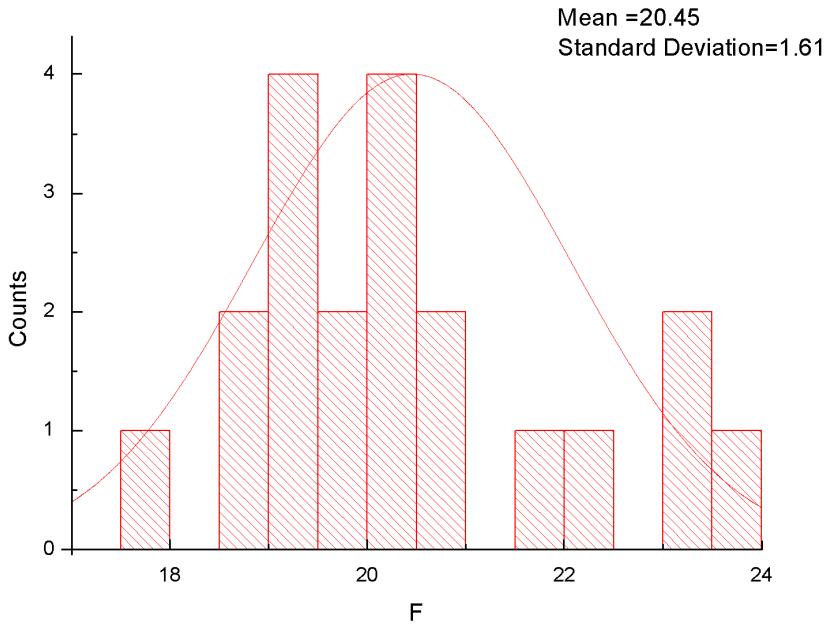

Figure 3.14: the statistics of F parameter

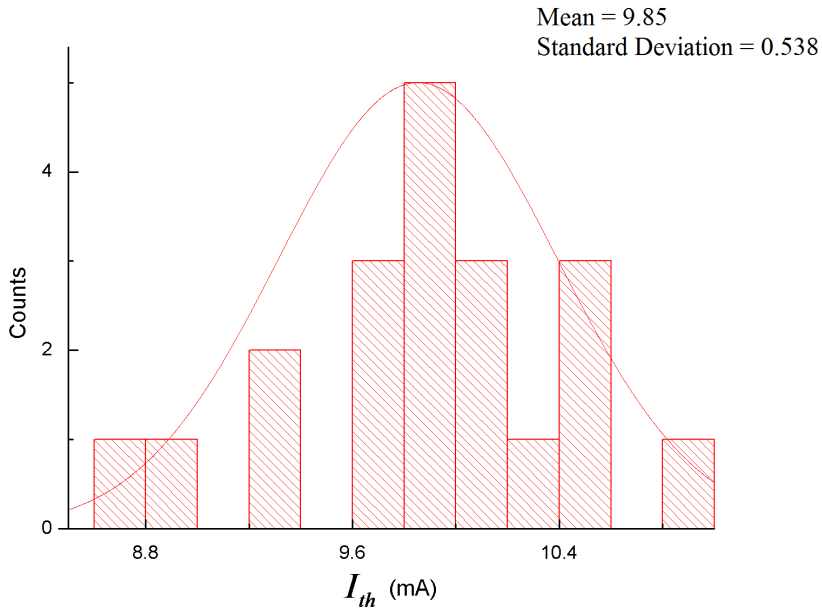

Figure 3.15: the statistics of I_{th} parameter

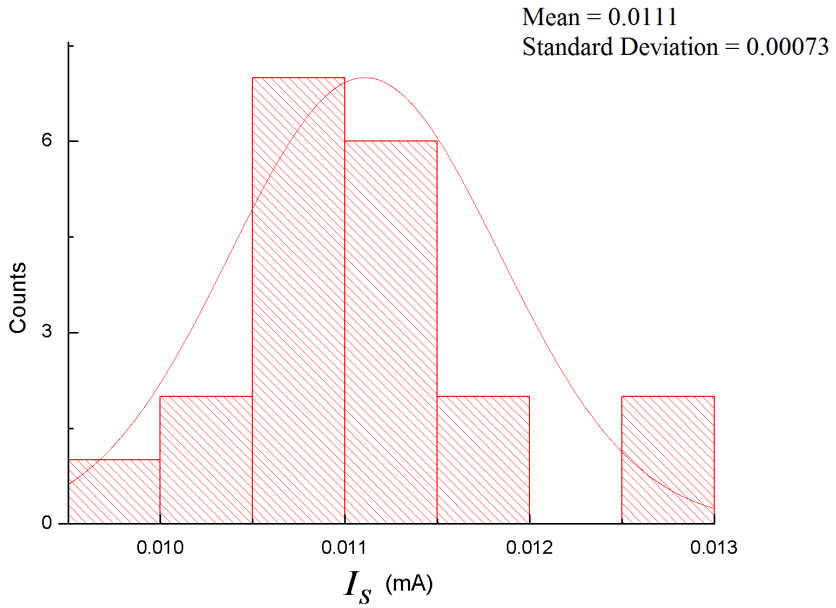

Figure 3.16: the statistics of I_S parameter

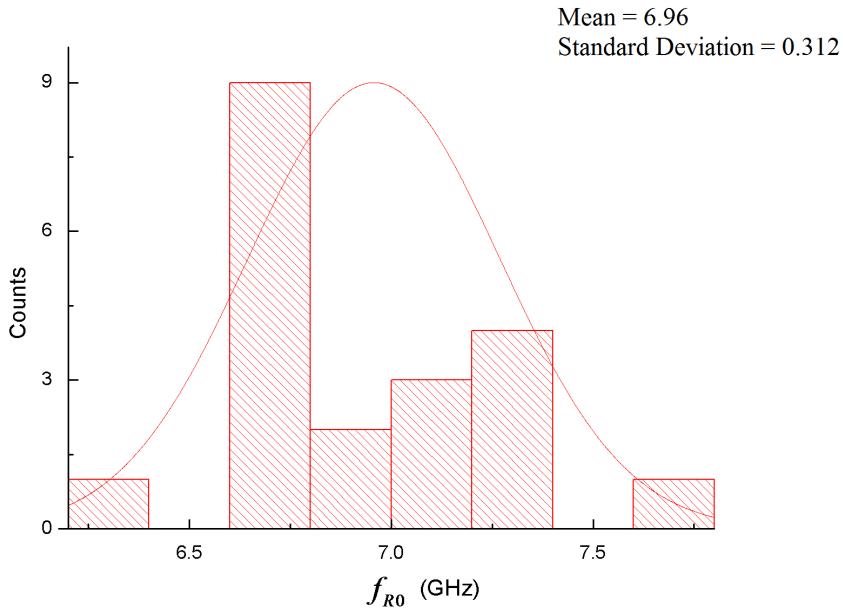

Figure 3.17: the statistics of f_{R0} parameter

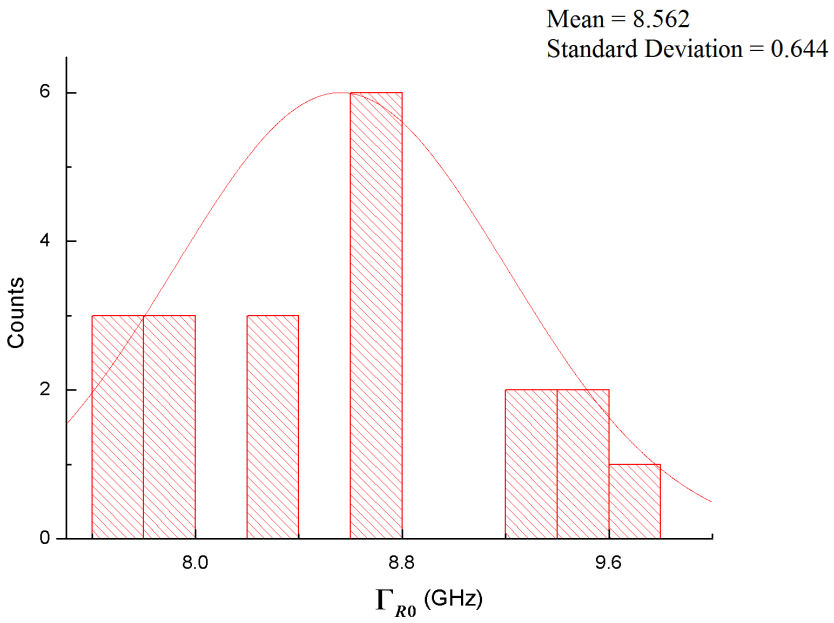

Figure 3.18: the statistics of Γ_{R0} parameter

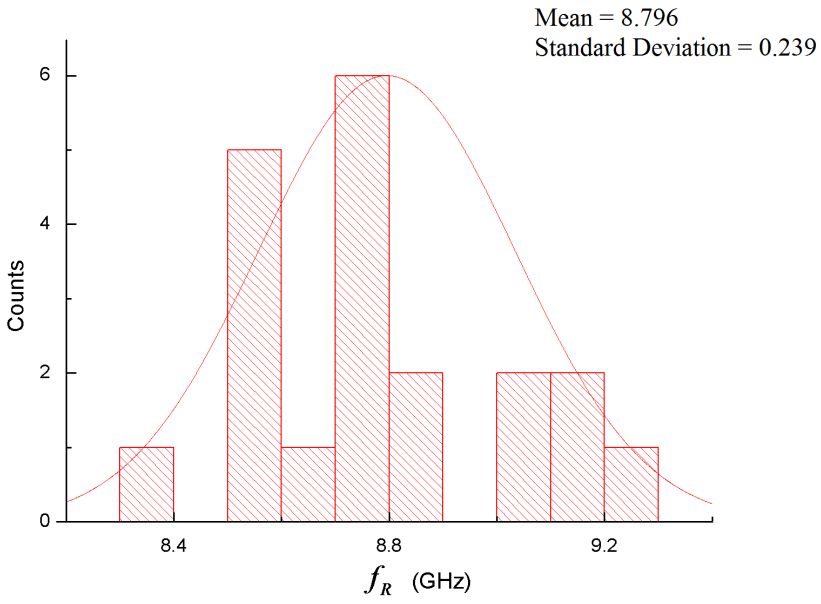

Figure 3.19: the statistics of f_R parameter

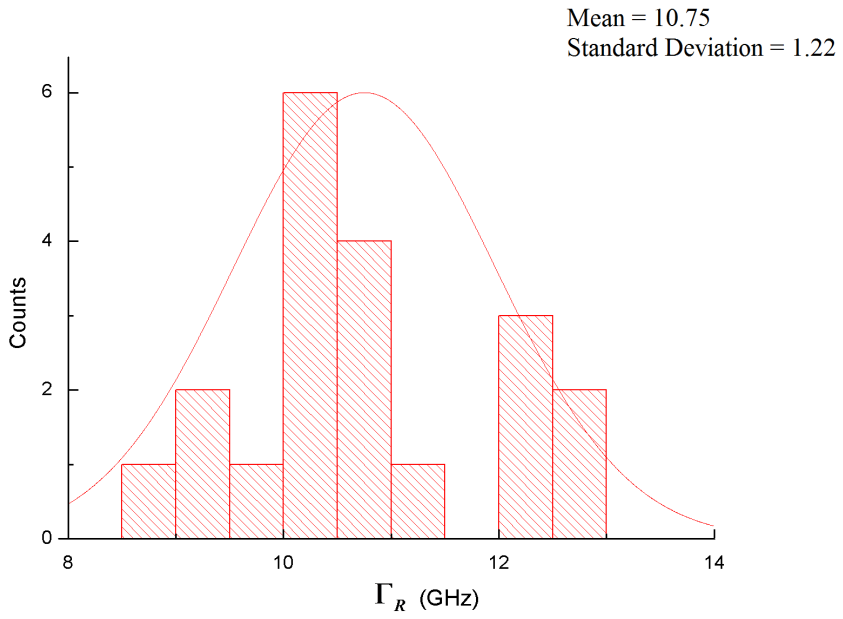

Figure 3.20: the statistics of Γ_R parameter

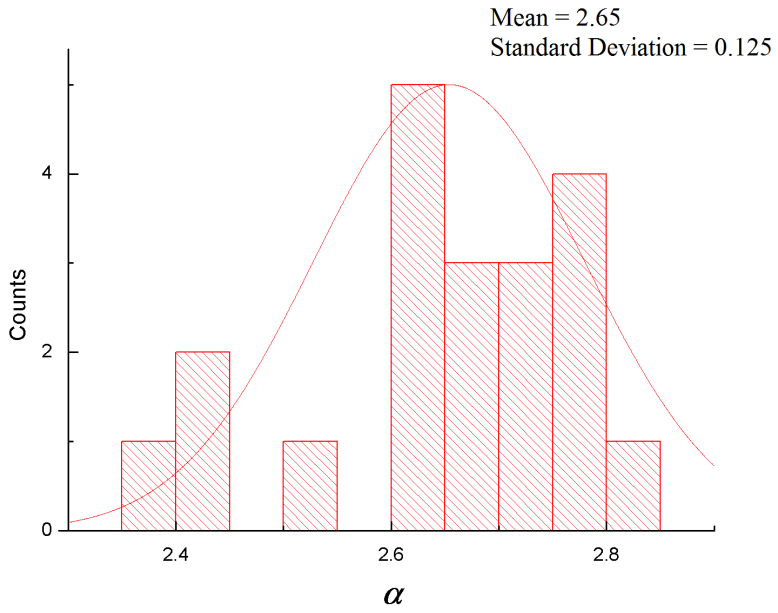

Figure 3.21: the statistics of α parameter

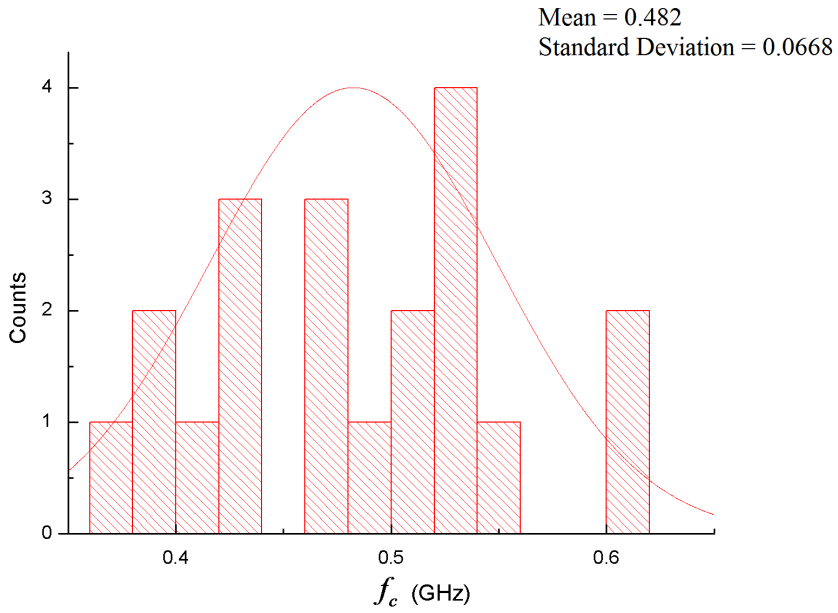

Figure 3.22: the statistics of f_c parameter

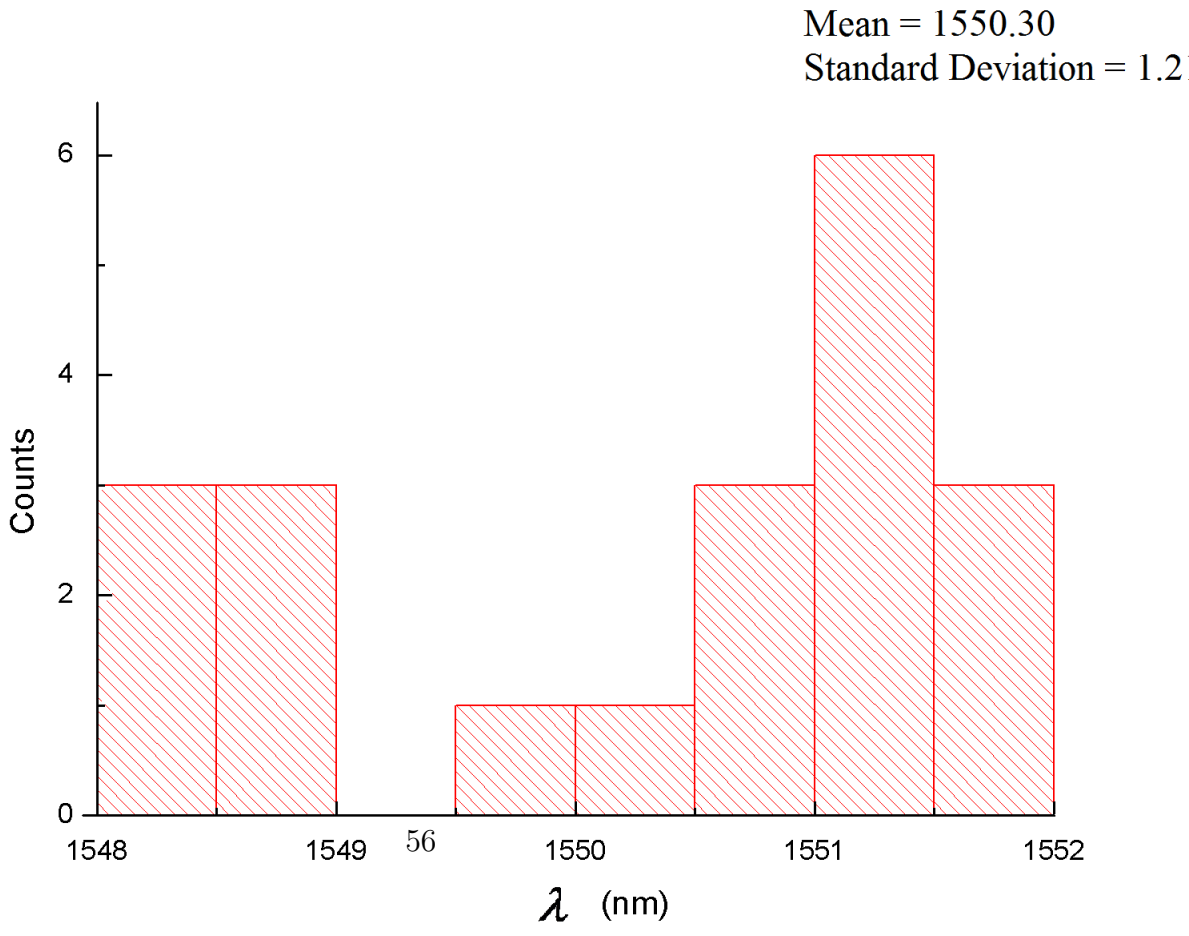

All diagram above shows a Gaussian (normal) distribution trend. The reason for imperfection of the statistics are due to the relative small sample size. With large sample size, these experimental data can be used as pre-knowledge of certain type of DFB laser, thus bring the following advantage :

1. A better initial value range for curve fitting process. Since the software that was developed for curve fitting utilize the least square error method, so the initial guess to be used are very important in terms of extraction process efficiency. With enough sampling, these initial value ranges can be utilized to speed up the extraction process.

2. A even better situation, with large amount of data, one can give a good approximation of DFB laser rate equation parameters without actually performing the experiment, when the type of DFB laser is known.

3.5 Calculation of the rate equation parameters from experimental data

By far, the parameters extracted from these experiments data introduced above are: F, I_{th}, I_S, Ω_{R0}, Γ_{R0},Ω_R, Γ_R α, F_D and ω_c. In this section, these experimental parameters will be calculated to yield the rate equation parameters.

The first step is using equations (2.44). with value of $q = 1.6021 \times 10^{-19}\ C$, $h = 6.625 \times 10^{-34}\ J \cdot S$, $c = 2.997925 \times 10^{8}\ m/s$, the measured wavelength of this particular laser is $\lambda = 1.54841 \times 10^{-6} m$ and the measured $F = 19.82925 J/s$. By substitute all these values into (2.44), yield the parameter $\eta = 0.125977402$.

The second step is to using equation (2.68). The value of Γ and V_{act} can be

assumed, they are in fact dummy parameters and their selection will not affect the results for the calculation of the output field from the direct modulated DFB lasers. The value to be picked for these two parameters are $\Gamma = 0.1$ and $V_{act} = 3 \times 10^{-17} m^3$ from article of publication [29]. Other parameters are $q = 1.6021 \times 10^{-19}\ C$, $I = 0.02\ A$, $I_{th} = 0.009672\ A$, $\Omega_{R0} = 7.3153315 \times 10^9 \times 2\pi\ rad/s$. The value of g_0 can be calculated by substitute above values into (2.68), which $g_0 = 9.831559349 \times 10^{-12} m^3/s \approx 9.8316 \times 10^{-12} m^3/s$

The third step is to utilize equation (2.82). The value of each know coefficients are $\omega_c = 5.065 \times 10^8 \times 2\pi rad/s$, $q = 1.6021 \times 10^{-19}\ C$, $I = 0.02\ A$, $I_{th} = 0.009672\ A$, $\Gamma = 0.1$ and $V_{act} = 3 \times 10^{-17} m^3$, then the value of ϵ is calculated as $\epsilon = 1.480996267 \times 10^{-23} m^3$.

The fourth step is to use equation (2.69). Here, both Ω_R and Ω_{R0}, Γ_R and Γ_{R0} values are utilized to solve τ_p and τ_c. With $\Omega_R = 9.1525 \times 10^9 \times 2\pi rad/s$,$\Gamma_R = 12.264 \times 10^9 \times 2\pi$, $\Omega_{R0} = 7.3153315 \times 10^9 \times 2\pi rad/s$ and $\Gamma_{R0} = 9.24 \times 10^9 \times 2\pi$. By re-arrange equation (2.69) yield:

$$\tau_p = \frac{2(\Gamma_R - \Gamma_{R0})}{\Omega_R^2 - \Omega_{R0}^2} \tag{3.12}$$

and

$$\tau_c = \frac{1}{2\Gamma_R - \frac{2(\Gamma_R - \Gamma_{R0})}{\Omega_R^2 - \Omega_{R0}^2} \cdot \Omega_R^2}\ . \tag{3.13}$$

By solving both equations (3.12) and (3.13), the value of τ_c and τ_p are found as$\tau_c = 2.569966757 \times 10^{-10} s$ and $\tau_p = 1.025472607 \times 10^{-12} s$, respectively.

The fifth step is by utilize equation (2.39). Since the value of g_0, τ_c and τ_p are known, then the value of β_{sp} can be calculated. The required parameters values are:

$I_S = 1.19709 \times 10^{-5} A$ $q = 1.6021 \times 10^{-19}$ C, $\Gamma = 0.1$, $V_{act} = 3 \times 10^{-17} m^3$, $g_0 = 9.831559349 \times 10^{-12} m^3/s$, $\tau_c = 2.569966757 \times 10^{-10} s$ and $\tau_p = 1.025472607 \times 10^{-12} s$, then rearrange (2.39), yield

$$\beta_{sp} = \frac{I_S g_0 \tau_c \tau_p \Gamma}{q V_{act}} \tag{3.14}$$

gets $\beta_{sp} = 6.45341958 \times 10^{-4}$.

The last step is to find N_0 by using equation (2.34). Given the following values of parameters: $I_{th} = 0.009672$ A, $\tau_c = 2.569966757 \times 10^{-10} s$,$q = 1.6021 \times 10^{-19}$ C, $\Gamma = 0.1$ and $V_{act} = 3 \times 10^{-17} m^3$, $g_0 = 9.831559349 \times 10^{-12} m^3/s$ and $\tau_p = 1.025472607 \times 10^{-12} s$, then rearrange (2.34), one gets

$$N_0 = \frac{I_{th} \tau_c}{q V_{act}} - \frac{1}{\Gamma g_0 \tau_p} \tag{3.15}$$

by substituting values into the above equation, yield,$N_0 = 4.747 \times 10^{23} m^{-3}$.

The list of extracted parameters for DFB laser rate equations is summarized in table 3.4.

3.6 Statistics of the Extracted Parameters

As expected, since the experimental data exhibited a Gaussian distribution trend, under linear transformation, the resulted parameters for the laser rate equations are also exhibit a Gaussian distribution trend:

Table 3.4: The extracted rate equation parameters.

parameters	values	units
Γ	0.1	
N_0	4.747×10^{23}	m^{-3}
τ_p	$1.025472607 \times 10^{-12}$	s
β_{sp}	$6.45341958 \times 10^{-4}$	
τ_c	$2.569966757 \times 10^{-10}$	s
V_{act}	3×10^{-17}	m^3
g_0	$9.831559349 \times 10^{-12}$	m^3/s
ϵ	$1.480996267 \times 10^{-23}$	m^3
η	0.125977402	
α	2.39	
λ	1548.41	nm

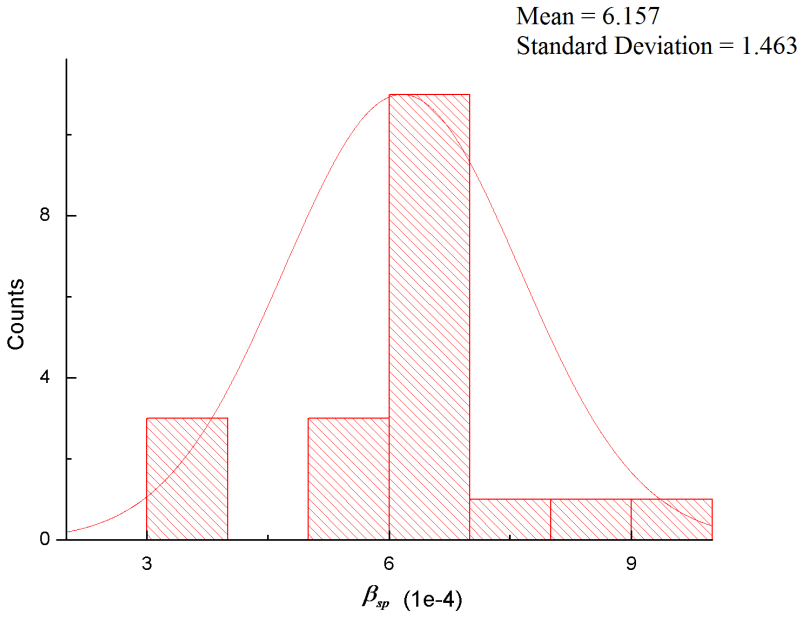

Figure 3.24: the statistics of β_{sp} parameter

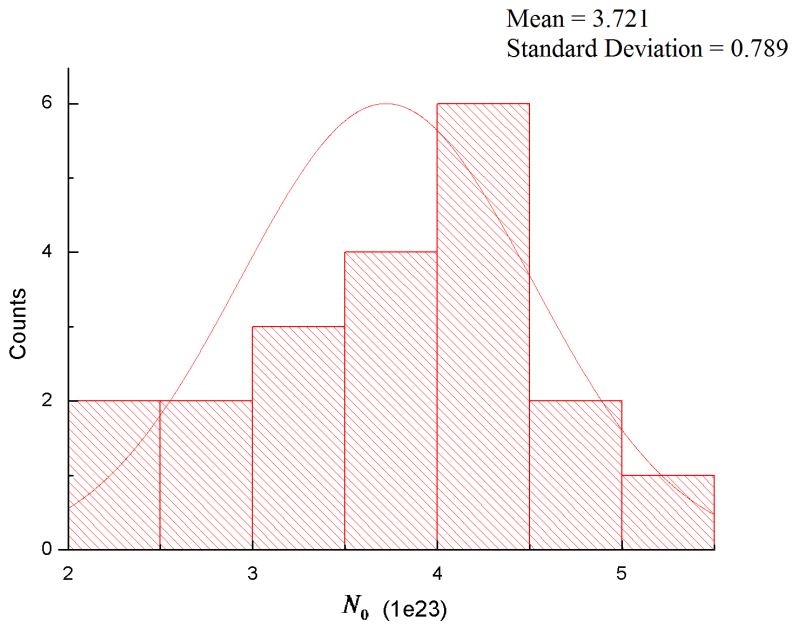

Figure 3.25: the statistics of β_{sp} parameter

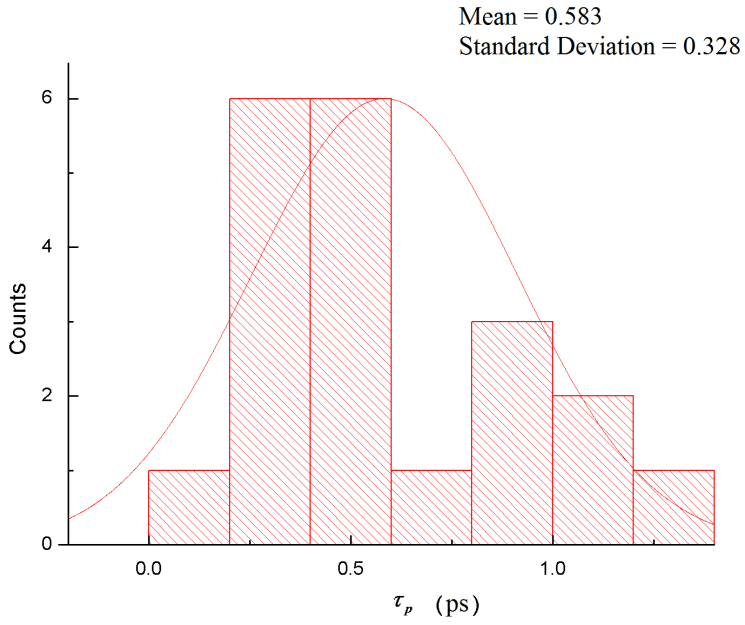

Figure 3.26: the statistics of τ_p parameter

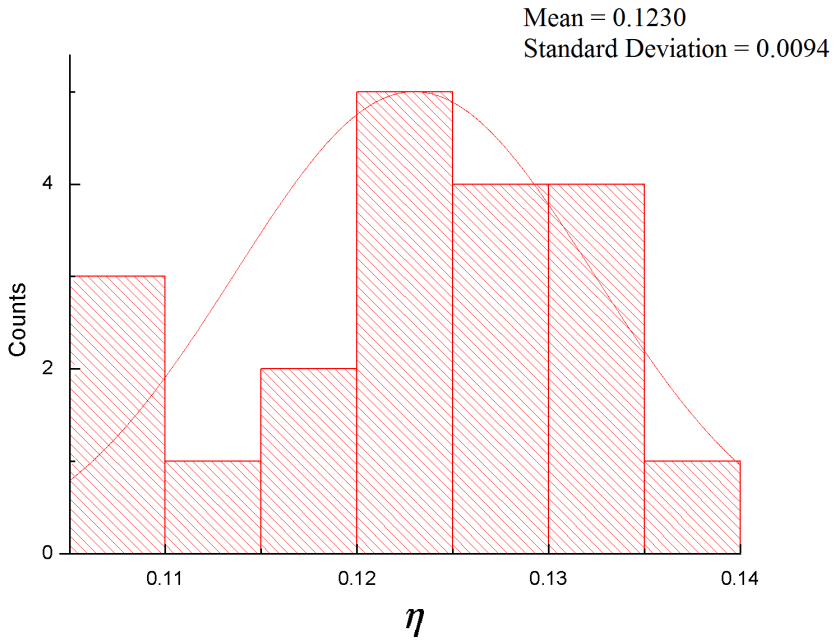

Figure 3.27: the statistics of η parameter

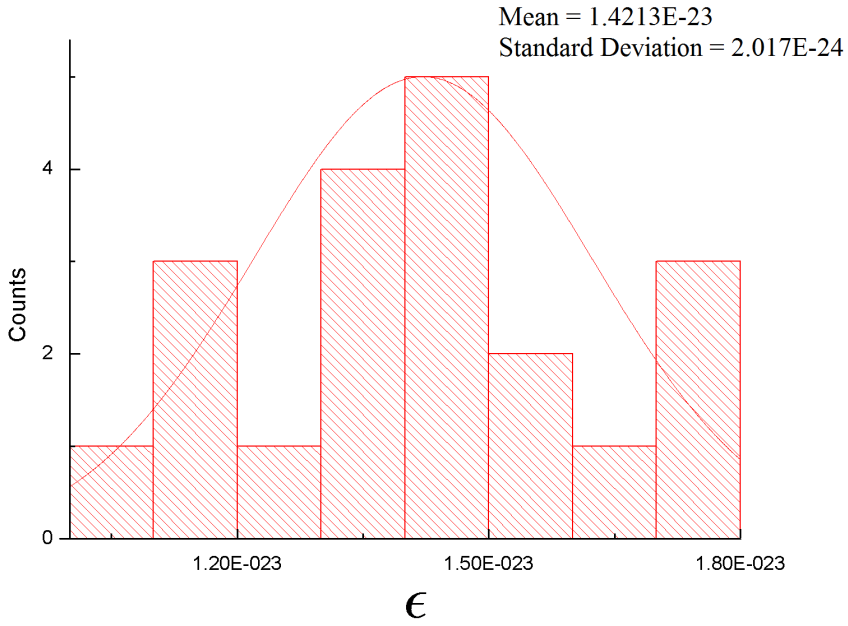

Figure 3.28: the statistics of ϵ parameter

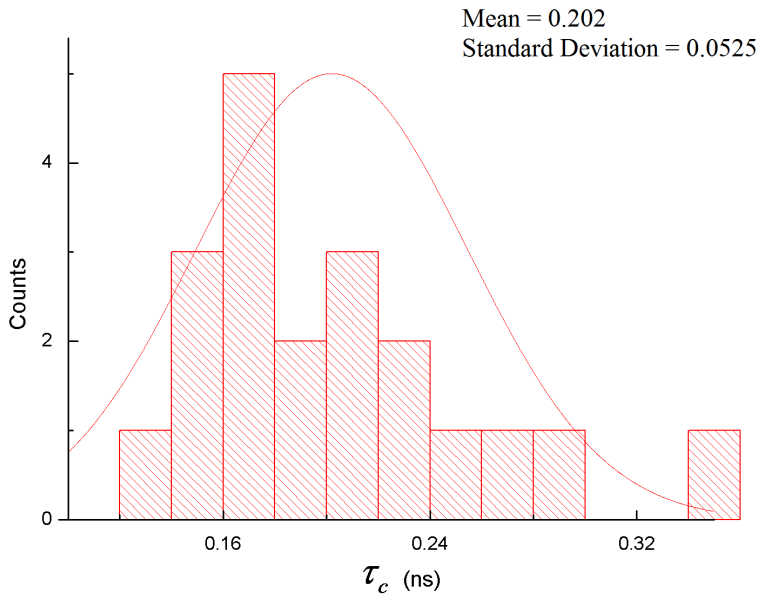

Figure 3.29: the statistics of τ_c parameter

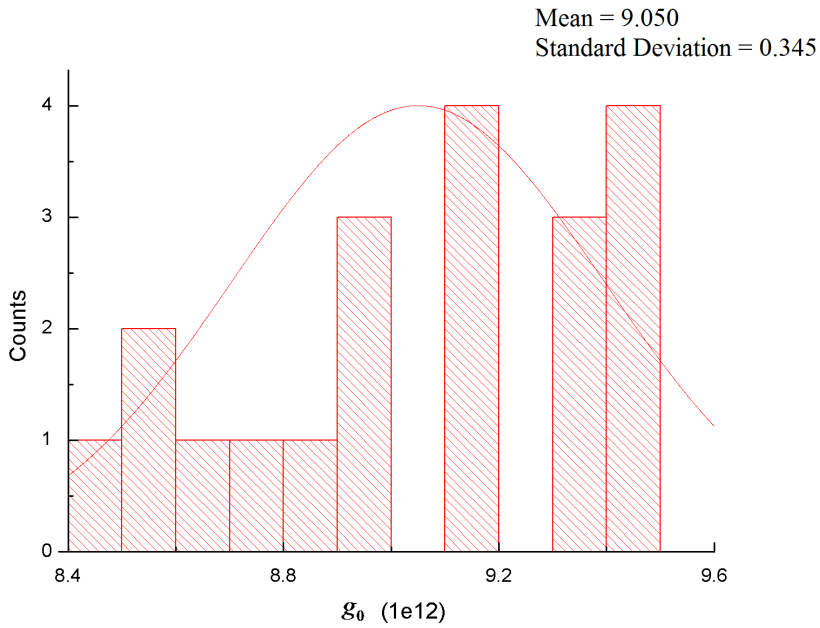

Figure 3.30: the statistics of g_0 parameter

With large sample size, these experimental data can be used as pre-knowledge of certain type of DFB laser, thus bring the following advantage :

1. A better initial value range for curve fitting process. Since the software that was developed for curve fitting utilize the least square error method, so the initial guess to be used are very important in terms of extraction process efficiency. With enough sampling, these initial value ranges can be utilized to fast the extraction process.

2. A even better situation, with large sample of data, one can give a good approximation of DFB laser rate equation parameters without actually performing the experiment, when the type of DFB laser is known.

Chapter 4

Extraction of the Line-width Enhancement Factor of DFB Semiconductor Lasers

4.1 Introduction

The semiconductor laser is a key component in the integrated optical circuit for high speed optical communication[30]. The frequency chirping of the semiconductor laser is one of the most important factors affecting the performance of the optical communication system [31]. The frequency chirping is mostly related with the line-width enhancement factor in the rate equations model [32, 33]. Therefore, it is important to extract the line-width enhancement factor accurately from measurement in order to optimize the performance of the communication system. Several methods have been proposed for chirp parameter extraction [20, 34–38]. The optical fiber dispersion method can be utilized to measure the line-width enhancement factor of laser diodes lasing around 1550 nm[37–39]. However it is not valid for those lasing around 1310 nm due to the low fiber dispersion at this wavelength. The FM (frequency modulation) to AM (amplitude modulation) conversion method can be employed to

extraction chirp parameter for laser diodes lasing around 1550 nm or 1310 nm[34, 35]. In this method both the FM index and IM (intensity modulation) index are required to be obtained before performing the curve fitting[20, 35]. However it is difficult to obtain FM index by keeping one specified sideband suppressed due to complicated manipulation and requiring a high resolution function generator. It is required to sweep modulation frequency in a wide range and high resolution. It is also not easy to obtain FM index by solving the transcendental side-band strengths ratio function numerically. Based on the measured data of FM to AM method, a new method is proposed in this paper to extract the chirp parameter by fitting the strength ratio curve of the first and the second sidebands. It only needs to measure the IM index at the beginning one time and avoids obtaining FM index. The chirp parameter extracting process is greatly simplified and can be done automatically by a computer.

4.2 The Proposed Method

The experimental set-up for single mode laser measurement is as shown in Fig 4.1, the laser diode is driven by a DC bias on ILXLightwave LDC-3900 modular on THORLABS LM9LP mount and a sinusoidal RF source which is gated by 2T period and 50% duty cycle. The single mode laser's signal is sent directly to the Mach-Zehnder interferometer, whose differential delay is T, after passing an isolator.

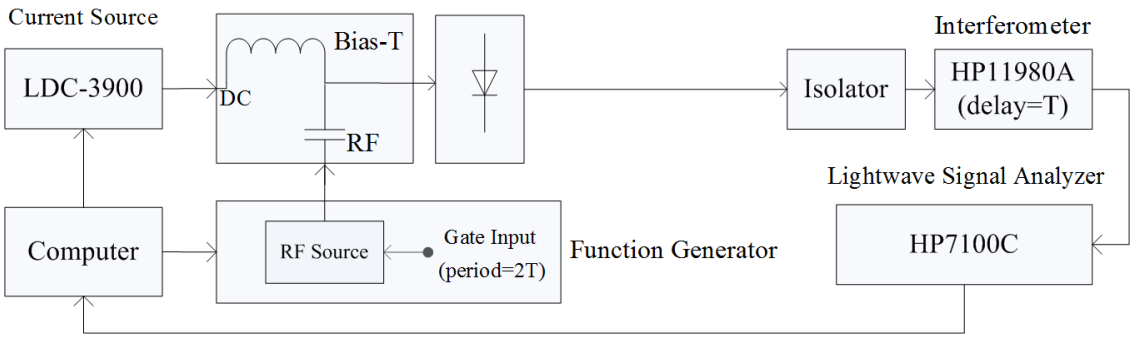

Figure 4.1: The experimental setup used in the purposed method.

If the modulation index is significantly small, the ratio of the first and second side-band strengths of the intensity spectrum measured by the light-wave signal analyzer is well described by the equation:

$$\frac{S_2}{S_1} = \frac{J_2^2(\beta)}{J_1^2(\beta)} \tag{4.1}$$

where S_1 and S_2 are the first and second side band strengths, respectively; J_n is the nth order Bessel function;β and m are FM and IM indices, respectively.

4.2.1 Relationship between intensity-modulation and frequency modulation

Since the carrier density inside the laser diode controls both the optical intensity and the optical emission frequency, it is useful to relate intensity modulation and the frequency modulation directly[40][41]. Such relations have been investigated in [34][42],both experimentally[43][44][45] and theoretically[35][46]. The optical intensity is proportional to the photon number, which is related to the carrier density via the

photon rate equation, which here use a more generalized rate equation (4.2).

$$\frac{dS}{dt} = \frac{S}{\tau_p}(G-1) + K_{tot}R_{sp} \tag{4.2}$$

with G is the normalized gain and K_{tot} is the enhancement factor of spontaneous emission. The normalized gain $G = R_{st}\tau_p$, with R_{st} represents stimulated emission rate, contains a linear and a nonlinear part according to equation (4.3)

$$G = G_L(1-\kappa P) = G_L(1-\kappa_s S) \tag{4.3}$$

with the linear gain G_L and the gain compression coefficient κ with respect to the optical power P per facet. And since G is very close to unity above threshold, even for large signal modulation, it may be expanded in terms of $N = N_{th}$, where N_{th} corresponds to the carrier density for which the linear gain G_L is unity, yielding

$$G = 1 + (\partial G/\partial N)(N - N_{th}) - \kappa_s S. \tag{4.4}$$

The photon rate equation (4.2) with $R_{sp} \approx N_{sp}/\tau p$ is then written as

$$\frac{dS}{dt} = \frac{S}{\tau_p}\left(\frac{\partial G}{\partial N}(N-N_{th}) - \kappa_s S\right) + K_{tot}N_{sp}/\tau_p. \tag{4.5}$$

Since $G = g v_g \tau_p$, we have

$$(\partial G/\partial N) = (\partial g/\partial N) v_g \tau_p \tag{4.6}$$

and with equation (4.7)

$$\frac{d\phi}{dt} = \frac{\alpha}{2} v_g \frac{\partial g}{\partial n}(N - N_{th}). \tag{4.7}$$

yields

$$2\pi(v - v_{th}) = \frac{\alpha}{2\tau_p} \frac{\partial G}{\partial N}(N - N_{th}). \tag{4.8}$$

In equation (4.5) the nonlinear gain has been introduced. However, the refractive index is assumed to be linear, depending only on the carrier density, so that the photon number S does not explicitly appear in equation (4.8). This assumption is supported by references [44][45] indicating that the nonlinear gain appears to be much more important than the nonlinear refractive index.

Equations (4.5) and (4.8) yield a direct relation between photon number S and optical frequency v according to[45]

$$v - v_{th} = \frac{\alpha}{4\pi} \left(\frac{d(ln\ S)}{dt} + \frac{1}{\tau_p}[\kappa_S S - K_{tot} N_{sp}/S] \right). \tag{4.9}$$

This is a very useful equation for several reasons. For a given intensity modulation, it predicts the related frequency modulation and thus the associated chirp. On the other hand the measured relation between intensity modulation and frequency modulation yields an estimate for the coefficient α and the gain compression coefficient κ_s [44][34].

So far, the analysis is somewhat oversimplified, since a uniform carrier reservoir is assumed. Actually, it turns out that the relation between frequency modulation and intensity modulation is not properly described by equation (4.9), if carrier density is either axially or laterally inhomogeneous [43]. These inhomogeneities are important, especially for GaAlAs lasers (exhibiting low nonlinear gain) with a laterally

inhomogeneous carrier profile, such as for example the CSP laser. Fortunately, even if inhomogeneities are taken into account the relation between intensity modulation and frequency modulation may still be described by equation (4.9), at least approximately, if the parameter κ_s is suitably adjusted [47]. Here the parameters κ and κ_s thus describe the combined effect of nonlinear gain and an inhomogeneous carrier distribution where κ_s, due to the inhomogeneities, may be either positive or negative.

If a small signal sinusoidal modulation of the photon number S is assumed according to

$$S =< S > +\Re(\Delta S \; exp(j\omega t)) \tag{4.10}$$

with $|\Delta S| <<< S >$ and ω denoting the angular modulation frequency, the frequency modulation may be written as

$$v =< v > +\Re(\Delta v \; exp(j\omega t)) \tag{4.11}$$

and equation 4.9 yields

$$\Delta v/\Delta S = \frac{\alpha}{4\pi < S >}(j\omega + \omega_c) \tag{4.12}$$

with

$$\omega_c = (\kappa_s/\tau_p) < S > +K_{tot}N_{sp}/(< S > \tau_p) \tag{4.13}$$

For low modulation frequencies the frequency modulation (FM) is simply proportional to the intensity modulation (IM) and this proportionality is governed by the characteristic frequency ω_c.

It is often more convenient to relate the FM-modulation index

$$\beta = |2\pi\Delta v/\omega| \tag{4.14}$$

to the IM-modulation index

$$m = |\Delta S/ < S > | \tag{4.15}$$

yielding [48]

$$\frac{\beta}{m} = \frac{\alpha}{2}\sqrt{1 + \frac{\omega_c^2}{\omega^2}} \tag{4.16}$$

where α is line-width enhancement factor, ω is the modulation frequency and ω_c is the chirp frequency. The FM index can be expressed by rearranging equation (4.16) as follows

$$\beta = \frac{\alpha m}{2}\sqrt{1 + \frac{\omega_c^2}{\omega^2}} \tag{4.17}$$

By substituting (4.17) into (4.1), the ratio of sideband strengths is described as

$$R(\omega) = \frac{S_2}{S_1} = \frac{J_2^2\left(\frac{\alpha m}{2}\sqrt{1 + \frac{\omega_c^2}{\omega^2}}\right)}{J_1^2\left(\frac{\alpha m}{2}\sqrt{1 + \frac{\omega_c^2}{\omega^2}}\right)} \tag{4.18}$$

The IM index m is measured at the beginning and fixed to a proper value satisfying the small signal modulation conduction. The side-band strengths ratio $R(\omega)$ becomes a function of modulation frequency ω with two parameters α and ω_c. A computer program is implemented to sweep the modulation frequency by controlling the

function generator and record the corresponding intensity spectrum from the lightwave signal analyzer. The side-band strengths ration curve is obtained by searching the first and second side-band strengths in each recorded intensity spectrum corresponding to each modulation frequency. By fitting the measured side-band strengths ratio curve with theoretical function (4.18), the line-width enhancement factor can be extracted easily.

4.3 Validation

The proposed method is verified in experiments by measuring a MQW DFB laser round 1550nm. The side-band strengths ratio curve is measured automatically by the computer program which sweeps the modulation frequency of the function generator and reads modulated frequency spectrum from the lightwave signal analyzer. When the side-band strengths ratios are obtained under different modulation frequencies, a fitting process is applied according to the theoretical equation (4.18), and the chirp parameter is extracted. As shows in Fig 4.2, the blue circles are measured data and the solid line is the best fit calculated from equation (4.18). The extracted alpha parameters for the DFB laser is 1.87 .

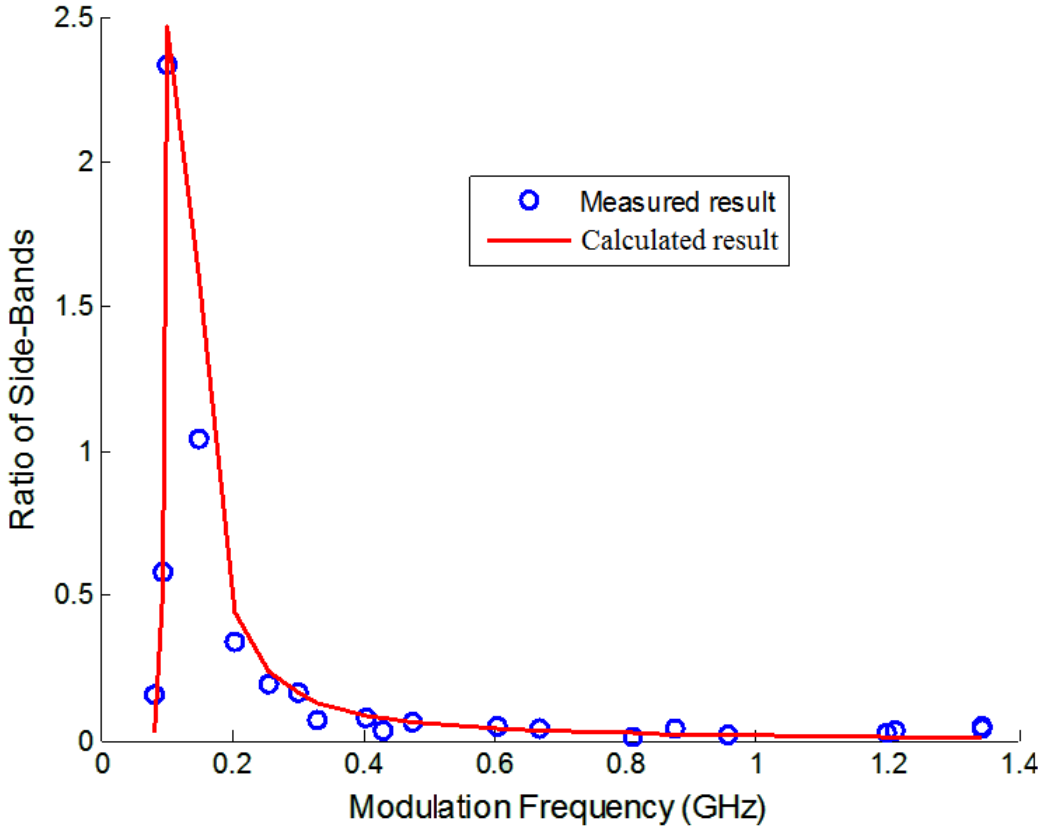

Figure 4.2: Measured (circle) and calculated (solid line) ratios of side-bands as a function of modulation frequency

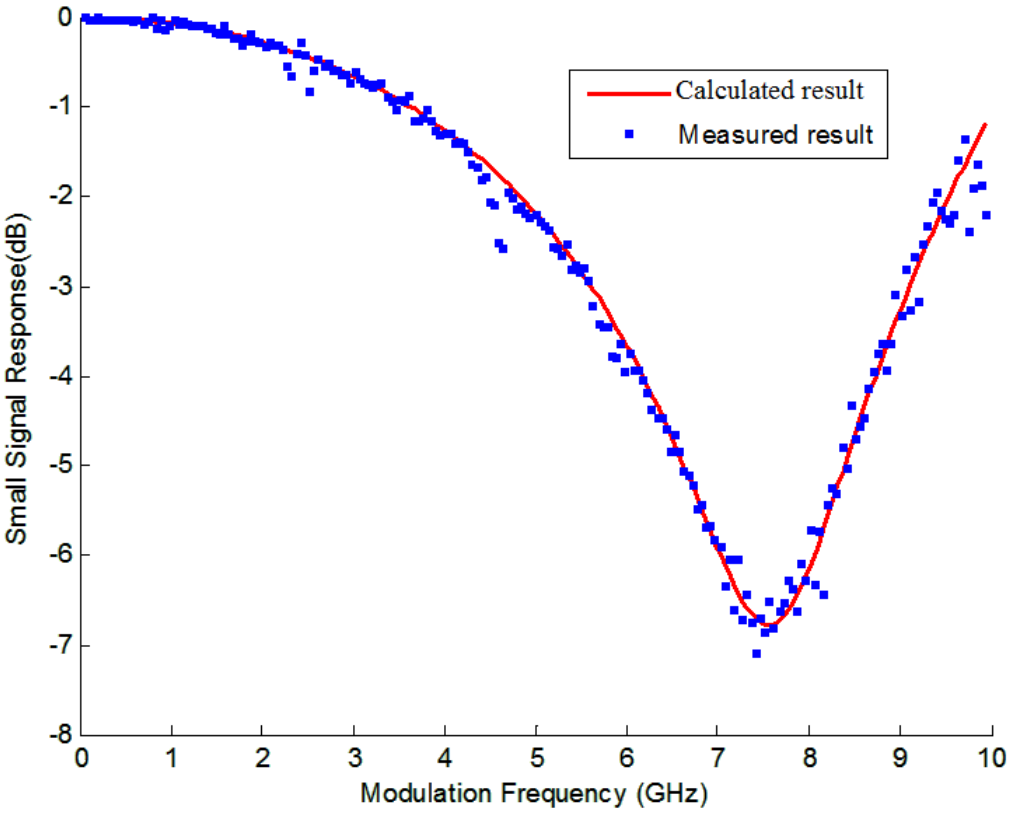

Figure 4.3: Measured (circle) and calculated (solid line) small signal response of a DFB laser with 25.3km SMF-28 fiber

To validate the method proposed, the widely adopted optical fiber dispersion method is chosen as a benchmark [37].

The light-wave signal generated by a DFB laser is not purely monochromatic. The spectrum of the output signal is located at a central frequency and has a certain line-width from several kilo-Hz to a couple of mega-Hz. While the DFB laser is directly modulated with injection current, the central frequency of the light-wave changes with the output power. This is called frequency chirping. The frequency chirping property causes the line-width of the light-wave even larger when the laser diode is modulated. When passing the chirped light-wave through a dispersive optical fiber, the carried signal is distorted and the output power through the optical fiber is affected. The small signal intensity modulation response is important to study the performance of a laser diode in an optical fiber system.

The input signal to the optical fiber is directly modulated laser diode with intensity modulation characteristic as:

$$\Delta S_{in}(j\omega) = \left(\frac{\tau_p}{q}\right) H(j\omega)\,\Delta I(j\omega) \ , \tag{4.19}$$

where

$$H(j\omega) = \frac{\omega_R^2}{(j\omega)^2 + 2j\Gamma_R\omega + \omega_R^2} \ . \tag{4.20}$$

The intensity modulation at the output of fiber is given by

$$\Delta S_{out}(j\omega) = \left[\cos\left(F_D\omega^2\right) - \alpha\left(1 - j\frac{\omega_c}{\omega}\right)\sin\left(F_D\omega^2\right)\right] \cdot \left(\frac{\tau_p}{q}\right) H(j\omega)\,\Delta I(j\omega) \ , \tag{4.21}$$

where the optical fiber transfer function is given by

$$\begin{aligned} H_{fiber,dB} &= \Delta P_{fiber,dB} - \Delta P_{LD,dBm} \\ &= 10 \times \log \left[\cos\left(F_D \omega^2\right) - \alpha \left(1 - j\frac{\omega_c}{\omega}\right) \sin\left(F_D \omega^2\right) \right] \ . \end{aligned} \tag{4.22}$$

The parameters are

$$F_{\mathrm{D}} = \frac{\lambda^2 D L_{fibre}}{4\pi c} \tag{4.23}$$

and

$$\omega_c = \frac{\varepsilon \Gamma}{eV} \left(I - I_{th}\right) \ , \tag{4.24}$$

with D is the dispersion coefficient and L_{fiber} is the length of the fiber.

This experimental setup to validate are as the following: semiconductor laser is powered by power supply ILXLightwave LDC-3900 modular laser diode controller and the small signal intensity modulation response is measured through Agilent 8703B Lightwave Component Analyzer. The current of the laser diode is directly modulated by an RF signal. The light-wave component analyzer modulate and sweep the frequency of all available bandwidth of the analyzer to the laser and measure the output power at each frequency in order to plot the small signal intensity modulation response with repeat at several bias currents. The Semiconductor lasers are mounted on THORLABS LM9LP mount and connect with the modulation signal from the Agilent 873B Lightwave Component Analyzer, and the THORLABS LM9LP mount also connect to the power supply. Both power supply and lightwave component analyzer are communicated through GPIB ports to the controlling PC, and an automation software have been developed to control the instruments and analysis the result. The collected data are in the form of different response curve at different bias curve.

Due to equation (3.9), the experiment consists of two parts: In part one, with no long fiber conditions that small signal IM response curve is measured directly. In part two, an extra SMF-28 fiber with length of 25.3 km is connected to the laser before it attach to the optical component analyzer. The schematic of part one is the same as the Small signal Intensity Modulation from last section as show in Figure 3.4. The part two schematic is shown in Figure 3.9

The extracted value is compared with the result obtained from the benchmark. Fig 4.3 depicts the measured small signal responses of the DFB lasers after the light-wave signal passing through a 25.3km SMF-28 fiber. From a curve fitting process, the linewidth enhancement parameters of the DFB lasers are obtained to be 1.83. The parameters agree well with the values extracted by the proposed method.

4.4 Conclusion

In this chapter a new method is proposed for extracting the DFB laser chirp parameter by fitting the side-band strengths ratio curve obtained from the spectrum measurement. A MQW DFB laser is measured and the chirp parameter is extracted. The extracted value agrees well with the result obtained from fiber dispersion measurement. It is important to mention that although this method is tested with a DFB laser lasing at 1550nm in C-Band, it is also valid for the DFB laser lasing around 1310nm in O-Band. This method is also suitable for automatic parameter extraction.

Chapter 5

Conclusion and Future Work

In this thesis, the experimental methods to extract the parameters of DFB semiconductor laser rate equations were introduced ,analyzed and compared. These results demonstrated Gaussian distribution that can be utilized in the future to give either the initial guess value for the curve-fitting process, or even predict the value of the parameters without preform of the actual experiment.

The purposed method to extract of line-width enhancement factor also brings a new way to extract the chirp parameters without using dispersive fiber, which opens a new door to extract the rate equation parameters for laser that lasing around $1310nm$. Its simplicity made it a ideal way to automate the extraction procedure, compared with IM small signal response through dispersive fiber that, requires the change of connection during experiment.

Some suggested work in th future are as follows:

1. Improvement of the curve fitting process. The current curve fitting process utilizes least square error method to find the experimental parameters. However, this method is not be the best way to extract these parameters. A suggested method is

Levenberg-Marquardt Method [49].

2. Enlarge the sample space of DFB laser under tests to 200 [50]. The limited budget prevent me from working with large sample space.With sample space enlarged to 200, a better estimation of the rate equation parameters can be yield.

Bibliography

[1] G.P.Agrawal, *Fiber-optic communication systems*. New York, NY: Wiley Interscience, 2002.

[2] H.Li and K.Iga, *Vertical cavity surface emitting laser devices*. Springer, 2001.

[3] F.P.Kapron, D. Keck, and R. Maurer, "Radiation losses in glass optical waveguides ," *Applied Physics Letters*, vol. 17, pp. 423–425, 1970.

[4] T.Miya, Y.Terunuma, T.Hosaka, and T.Miyashita, "Ultimate low-loss single-mode fiber at 1.55Am," *Electronics Letters*, vol. 15, pp. 106–108, 1979.

[5] X. Li, *Optoelectronic devices: design, modeling, and simulation*. Cambridge University Press, 2009.

[6] J.L.Gimlett, B. Red, and N.K.Cheung, "Effects of phase-to-intensity noise conversion by multiple reflections on gigabit-per-second dfb laser transmission systems," *Journal of Lightwave Technology*, vol. 7, pp. 888–895, 1989.

[7] M. Geert and V. Patrick, *Handbook of distributed feedback laser diodes*. Lavoisier, 1997.

[8] H. D. Kim, S.-G. Kang, and C.-H. Le, "A low-cost wdm source with an ase injected fabry-perot semiconductor laser," *IEEE Photonics Technology Letters*, vol. 12, pp. 1067–1069, 2000.

[9] D. Yang, *Investigation of high-speed long-haul fiber-optic transmission*. McMaster University, 2006.

[10] D. M. Sullivan, *Electromagnetic simulation using the fdtd method*. IEEE Press, 2000.

[11] R. HU, *Finite element methods : an introduction* . M. Dekker, 1984.

[12] J. V. Roey, J. van der Donk, and P. E. Lagasse, "Beam-propagation method: analysis and assessment," *Journal of the Optical Society of American*, vol. 71, pp. 803–810, 1981.

[13] D. C. Witte, *The pseudospectral method for simulating wave propagation*. Columbia University, 1989.

[14] R.A.Saunders, J.P.King, and I.Hardcastle, "Wideband chirp measurement technique for high bit rate sources," *Electronic Letters*, vol. 30, pp. 1336–1338, 1994.

[15] J.C.Cartledge, "Improved transmission performance resulting from the reduced chirp of a semiconductor laser coupled to an external high-Q resonator," *J. Lightwave Technol.*, vol. 8, pp. 716–721, 1990.

[16] R.Schatz, E.Berglind, and L.Gillner, "Parameter extraction from DFB lasers by means of a simple expression for the spontaneous emission spectrum," *IEEE Photon. Technol. Lett.*, vol. 6, pp. 1182–1184, 1994.

[17] G.Morthier, K.Sato, R.Baets, T.K.Sudoh, Y.Nakano, and K.Tada, "Parameter extraction from subthreshold spectra in cleaved gain- and index-coupled DFB LDs," *Proc. Conf. Optical Fiber Communication*, pp. 102–104, 1995.

[18] L.V.T.Nguyen, A.J.Lowery, P.C.R.Gurney, and D.Novak, "A time-domain model for high-speed quantum-well lasers including carrier transport effects," *IEEE J. Select. Topics Quantum Electron*, vol. 1, pp. 494–504, 1995.

[19] J. C.Cartledge and R.C.Srinivasan, "Extraction of dfb laser rate equation parameters for system simulation purposes," *Journal of Lightwave Technology*, vol. 15, pp. 852–860, 1997.

[20] L. Bjerkan, A. Royset, L. hafsker, and D. Myhre, "Measurement of laser parameters for simulation of high-speed fiberoptic systems," *Journal of Lightwave Technology*, vol. 14, pp. 839–850, 1996.

[21] A. Bacou, A. Hayat, V. Iakovlev, A. Syrbu, A. Rissons, J.-C. Mollier, and E. Kapon, "Electrical modeling of long-wavelength vcsels for intrinsic parameters extraction," *Journal of Quantum Electronics*, vol. 46, pp. 313–322, 2010.

[22] L.M.Zhang and J.E.Carroll, "Large-signal dynamic model of the DFB laser," *IEEE J. Quantum Electron*, vol. 28, pp. 604–611, 1992.

[23] R.Schatz, E.Berglind, and L.Gillner, "High-speed modulation of semiconductor lasers," *J. Lightwave Technol.*, vol. LT-3, pp. 1180–1192, 1985.

[24] J. Hong, W.-P.Huang, and T.Makino, "Static and dynamic simulation for ridge-waveguide MQW DFB lasers," *IEEE J. Quantum Electron*, vol. 31, pp. 49–59, 1995.

[25] P.A.Morton, T.Tanbun-Ek, R.A.Logan, A.M.Sergent, P. Jr., and D.L.Coblentz, "Frequency response subtraction for simple measurement of intrinsic laser dynamic properties," *IEEE Photon. Technol. Lett.*, vol. 4, pp. 133–136, 1992.

[26] C.Harder, J.Katz, S.Margalit, J.Shacham, and A.Yariv, "Noise equivalent circuit of a semiconductor laser diode," *Journal of Quantum Electronics*, vol. 18, pp. 333–337, 1982.

[27] T. Morishita and J. Nishizawa, "Impedance characteristics of double-hetero structure laser diodes," *Solid State Electron*, vol. 22, pp. 951–962, 1979.

[28] R.C.Srinivasan and J.C.Cartledge, "On using fiber transfer functions to characterize laser chirp and fiber dispersion," *IEEE Photon. Technol. Lett.*, vol. 7, pp. 1327–1329, 1995.

[29] A. S.Karar, J. C.Cartledge, J. Harley, and K. Roberts, "Electronic precompensation for a 10.7-gb/s system employing a directly modulated laser," *Journal Of Lightwave Technology*, vol. 29, pp. 2069–2076, 2011.

[30] L. Han, Y. Wen, and W. Huang, "Automatic extraction of chirp parameter of dfb laser," *Optical Society of American Conference on Slow and Fast Light*, vol. 15, pp. 106–108, 2011.

[31] Y. Kim, H. Lee, J. Lee, J. Han, T. W. Oh, and J. Jeong, "Chirp characteristics of 10-gb/s electroabsorption modulator integrated dfb lasers," *IEEE Journal of Quantum Electronics*, vol. 36, pp. 900–908, 2000.

[32] I. Tomkos, I. Roudas, R. Hesse, N. Antoniades, A. Boskovic, and R. Vodhanel, "Extraction of laser rate equations parameters for representative simulations of

metropolitan-area transmission systems and networks," *Optics Communications*, vol. 194, pp. 109–129, 2001.

[33] C. H.Henry, "Theory of the linewidth of semiconductor lasers," *IEEE Journal of Quantum Electronics*, vol. 18, pp. 259–264, 1982.

[34] C. Harder, K. Vahala, and A. Yariv, "Measurement of the linewidth enhancement factor α of semiconductor lasers," *Applied Physics Letters*, vol. 42, pp. 328–330, 1983.

[35] R. Schimpe, J. Bowers, and T. Koch, "Characterization of frequency response of 1.5 m InGaAsP dfb laser diode and ingaas pin photodiode by heterodyne measurement technique," *Electronics Letters*, vol. 22, pp. 453–454, 1986.

[36] D. Baney and W. Sorin, "Measurement of a modulated dfb laser spectrum using gated delayed self-homodyne technique," *Electronics Letters*, vol. 24, pp. 669–670, 1988.

[37] A. Royset, L. Bjerkan, D. Myhre, and L. Hafskjaer, "Use of dispersive optical fibre for characterization of chirp in semiconductor lasers," *Electronics Letters*, vol. 30, pp. 710–712, 1994.

[38] K.Czotscher, S.Weisser, A.Leven, and J.Rosenzweig, "Intensity modulation and chirp of $1.55\mu m$ multiple-quantum-well laser diodes: modeling and experimental verification," *IEEE Journal of Selected Topics in Quantum Electronics,*, vol. 5, pp. 606–612, 1999.

[39] J.Wang and K.Petermann, "Small signal analysis for dispersive optical fiber communication systems ," *Journal of Lightwave Technology*, vol. 10, pp. 96–100, 1992.

[40] A.S.Sudbo, "The frequency chirp of current modulated semiconductor diode lasers," *IEEE J. of Quant. Electron*, vol. 22, pp. 1006–1008, 1986.

[41] O.Doyle, "Measuring Modulus and phase of chirp/modulated power ratio," *Electronics Letters*, vol. 23, pp. 133–134, 1987.

[42] T.L.Koch and J.E.Bowers, "Nature of wavelength chirping in directly modulated semiconductor lasers," *Electronics Letters*, vol. 20, pp. 1038–1040, 1984.

[43] O.Nilsson and Y.Yamamoto, "Small-signal response of a semiconductor laser with inhomogeneous linewidth enhancement factor: possibilities of a flat carrier-induced FM response," *Applied Physics Letters*, vol. 46, pp. 223–225, 1985.

[44] C.B.Su, V.Lanzisera, and R.Olshansky, "Measurement of nonlinear gain from FM modulation index of InGaAsP lasers ," *Electronics Letters*, vol. 21, pp. 893–895, 1985.

[45] T.L.Koch and R.A.Linke, "Effect of nonlinear gain reduction on semiconductor laser wavelength chriping," *Applied Physics Letters*, vol. 48, pp. 613–615, 1986.

[46] K.Kikuchi, T.Fukushima, and T.Okoshi, "Frequency-modulation characteristics of semiconductor lasers: deviation from theoretical prediction by rate equation analysis," *Electronics Letters*, vol. 22, pp. 453–454, 1986.

[47] W.Harth, "Quasistatic carrier induced frequency chirp in semiconductor laser diodes," *Arch. Elektr. Ubertr*, vol. 41, pp. 180–182, 1987.

[48] K. Petermann, *Laser diode modulation and noise*. Dordrecht: Kluwer Academic Publishers, 1988.

[49] W. H.Oress, S. A.Teukolsky, W. T.Vetterling, and B. P.Flannery, *Numerical recipes in c: the art of scientific computing*. Cambridge University Press, 2002.

[50] D. S.Yates, D. S.Moore, and D. S.Starnes, *The practice of statistics*. W.H.Freeman, 2007.